Chapter 8

Fiber Grating Lasers and Amplifiers

The arrival of the in-fiber Bragg grating could not have been at a better time for rare-earth-doped fiber. Research and development in the field of doped fibers was at such a stage that fiber amplifiers were already commercially available; thus, fiber Bragg gratings were a natural progression for combining the attributes of the fibers and amplifiers, as well as semiconductor devices. Their success in this area are due to the near-perfect reflection characteristics of the grating and the ultralow insertion loss, as well as the ease with which they can be tailored for a particular application. One of the most attractive features of the in-fiber Bragg grating is its transparency to wavelengths outside of the band stop. Apart from becoming integral components of narrow-band lasers, the side-tap filter and the long-period grating have also been particularly useful for equalizing the gain of optical fiber amplifiers. This chapter introduces some of the applications of fiber gratings in narrow-band, low-chirp lasers and mode-locked, short-pulse sources, as well as in tailoring the gain and stability of amplifiers.

8.1 Fiber grating semiconductor lasers: The FGSL

Semiconductor laser diode technology has been refined to produce low-threshold, high-power and narrow-linewidth devices (distributed feedback

lasers for a large number of applications [1]. The linewidth may be further narrowed by the use of a long external cavity. This technique has attracted much attention over the years [2]. Early work showed that while there was a benefit in line-narrowing from the linewidth enhancement factor of long external cavities, the instabilities were thought to be too difficult to overcome. In particular, reflections from intracavity elements such as the residual front facet reflections greatly affected the performance of the laser, except in the case of strong coherent feedback [3]. Much of the earlier work was limited to weak feedback due to in- and out-coupling losses to the external cavity. Wyatt and Devlin demonstrated line-narrowed (10 kHz) tunability over 55 nm in an InGaAsP 1.5-μm laser, using a bulk diffraction grating as the external cavity frequency selective mirror [4]. A semiconductor laser integrated with an etched Bragg reflector in a waveguide demonstrated the possibility of a compact configuration [5]. The fiber Bragg grating thus became the next obvious choice for an external reflector owing to its narrow bandwidth, with the possible advantage of defining the lasing wavelength and the potentially low coupling loss. Destroying the front facet reflectivity of a semiconductor laser and replacing it with a narrow-band fiber Bragg grating as an external cavity reflector is probably the worst possible configuration for making a high-quality laser. First of all, the semiconductor chip with cleaved facet mirrors forms an ultralow-loss cavity, since the mirrors are an integral part of the laser gain medium. Secondly, the laser semiconductor chip alone forms the shortest gain cavity, reducing the roundtrip time to a minimum and thereby allowing direct high-speed modulation. Thirdly, the high reflectivity of the output facet of the laser (~33%) is broadband; any external reflections returning to the laser, other than at the lasing wavelength, are attenuated equally, reducing the possibility of destabilizing laser operation. On the other hand, the fiber Bragg grating external-cavity semiconductor laser has several major limitations. The output facet reflectivity of the laser chip has to be reduced to low levels. The addition of a fiber in the cavity requires good coupling and low residual subcavity reflections in order to reduce intracavity losses and poses negligible return loss to wavelengths other than within the bandwidth of the Bragg grating. The cavity length increases correspondingly by the incorporation of a reflective Bragg element at some point within the fiber, increasing the cavity roundtrip time. What has the FGSL (or FGL) to offer to make it worth pursuing?

First, the fiber Bragg grating has a temperature coefficient [6] of wavelength change ~6–8 times lower than that of a semiconductor laser,

potentially increasing the wavelength stability of the laser in a hybrid configuration. Second, fiber Bragg gratings can be routinely fabricated at precise wavelengths and are therefore suited to mass production; wavelength control makes them useful for wavelength division multiplexing (WDM) applications that require extremely tight tolerances [7]. Third, the longer laser formed by the incorporation of the external cavity reduces the linewidth in direct relation to the length [8]. Fourth, semiconductor lasers suffer from chirp as a result of cavity length change during direct modulation. The longer FGSL dilutes the carrier induced cavity length change in the semiconductor during modulation, by confining it to the much smaller fraction of the laser length.

It is usual to quantify the operational sensitivity of a semiconductor laser by the linewidth enhancement factor α as [9,10]

$$\alpha = -\frac{4\pi}{\lambda}\frac{dn/dN}{dg/dN}, \tag{8.1.1}$$

where λ is the lasing wavelength, dn is the change in the refractive index of the laser, and dg/dN is the differential gain. In a semiconductor laser, the change in the gain and the refractive index is over the entire length of the laser L_s. With an extended cavity in which only part of the cavity is active, the influence of both these quantities is limited, with the result that the effect of the refractive index change (on the cavity length) is diluted.

The change in the laser wavelength $\delta\lambda$ as a function of injected carriers is given by

$$\delta\lambda = \lambda\frac{\partial l_{carrier}}{L_{laser}}, \tag{8.1.2}$$

where $\partial l_{carrier}$ is the change in the optical length of the semiconductor with injected current, and λ is the lasing wavelength. The inverse dependence of the shift in the wavelength on the laser cavity length demonstrates the advantage of the longer cavity [11].

Further, the wide gain bandwidth of the semiconductor chip in conjunction with a fiber Bragg grating used to define the operating wavelength can increase the yield, potentially allowing the use of *all* chips on a wafer. This becomes especially important with the tight specification for WDM system wavelengths. Semiconductor production technology of DFB lasers requires that each laser be measured for wavelength prior to packaging and consequently has implications for the replacement of faulty

lasers in WDM systems, where stocks may need to be maintained for each laser. The concept of retaining a fiber grating as part of the transmitter card, while replacing only the active gain medium when faulty, may have a cost advantage by reducing stocks. Finally, for telecommunications and sensor applications, lasers need to be pigtailed after fabrication. If the fiber grating is allowed to define the lasing wavelength, the two functions of operating wavelength and pigtailing may further reduce fabrication/packaging costs. These advantages are considered worthwhile to overcome the difficulties involved in optimizing laser chip-to-fiber coupling.

The first semiconductor laser to use an external cavity of an etched in-fiber Bragg grating was reported by Brinkmeyer *et al.* [12]. This laser used a standard uncoated Fabry–Perot fiber pigtailed laser chip operating at 1.3 microns, which was fusion spliced to an etched fiber grating, forming 2-meter-long cavity. With the twin coupled cavities (laser chip and laser chip with fiber grating), single-frequency operation of the laser was demonstrated with a linewidth of ~50 kHz. The narrow bandwidth of the grating (26 GHz) was much less than the FP mode spacing (140 GHz), although the long cavity longitudinal mode spacing was only 50 MHz. The reflectivity of the front facet of the FP laser $\rho_{FP} \approx 32\%$, while the reflectivity ρ_{fbg} of the grating is very low, ~0.01%; however, the combined coupled cavities results in a constructive interference with a contrast ratio of

$$|\rho_{FP} + \rho_{fbg}|^2/|\rho_{FP} - \rho_{fbg}|^2 \approx 1.07, \tag{8.1.3}$$

so that when the cavity length is tuned for constructive interference, the modes of the long fiber cavity have a differential gain that is higher than the FP laser modes. This demonstration showed that the selectivity and additional reflectivity of the external cavity grating have a beneficial effect even in such a simple configuration. Etched gratings in fibers as external cavity mirrors have also been used with 1500-nm diodes [13].

Morey *et al.* [14] showed the use of a photoinduced fiber Bragg grating with a semiconductor laser to operate at the grating wavelength of 820 nm. A schematic of the FGSL device is shown in Fig. 8.1. An antireflection-coated (~0.5% reflectivity) FP GaInAsP/InP buried-heterostructure 1.5-μm laser chip is coupled with a lensed fiber with a narrowband reflection grating spliced to it to form the external resonator [15]. The lensed fiber is aligned to maximize the output coupling and welded in place. This laser demonstrates a low chirp, which is restricted by the limited bandwidth

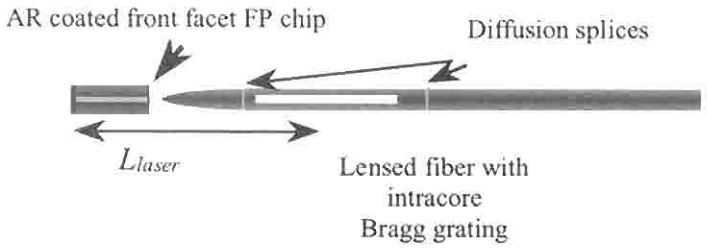


Figure 8.1: The external fiber grating semiconductor laser with an AR-coated FP chip coupled to a lensed fiber [3]. The measured chirp was instrument limited to be <0.5 MHz when modulated with NRZ pulses at 1.2 Gb/sec [15].

of the grating and the reduced change in the cavity length according to Eq. (8.1.2).

The linewidth of the laser for the 60-mm-long cavity was measured to be <50 kHz. The bias current varied between the threshold of 30 mA and 150 mA, changed the operating wavelength by <0.1 nm. The package temperature was controlled to ±5°C. A potentially low-cost FGSL operating at 1.3 μm with ~1 mW output power with an operating wavelength change of only 2 nm, over a temperature range of 100°C, has also been reported [16] for Access networks at 622 Mb/sec transmission rates.

The intracavity interference effects cause the modes of the laser to hop. This has been observed in experiments with FGSLs [11]. It was shown that as the lensed end of the external cavity fiber is moved away from the AR coated facet of the laser, the laser output drops until it stops lasing in a cyclic manner. These experiments showed the importance of the phase of the reflected light entering the cavity. If the free spectral range of the subcavity of the semiconductor is much larger than that of the external grating reflector, then the laser wavelength mode will pull within the grating bandwidth. The differential gain between the different external fiber grating cavity modes determines which wavelength lases at any one time. Changing the length of the cavity is similar to changing the bias current, and therefore requires some mechanism to compensate this effect.

In an effort to counter the detrimental effects of the variation of the phase as a function of bias current or modulation in the FGSL, a variation in the design using a chirped external grating reflector may be used, as is shown in Fig. 8.2 [17,18].

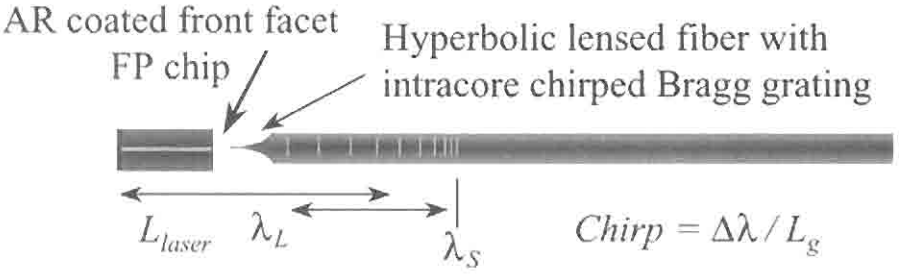


Figure 8.2: The chirped external fiber grating cavity laser [17]. The special AR-coated hyperbolic lens on the end of the fiber provides high-efficiency coupling of >98% [19], which in turn allows stable single-mode operation over a large output power (15 mW).

The principle of operation of chirped grating is to compensate for the current induced change in the optical cavity length of the semiconductor. As the length of the semiconductor cavity changes by δl_s to maintain an integral number of periods within the laser cavity, the wavelength shifts, altering the cavity length. In principle, the wavelength should shift smoothly as the bias current is altered.

In this case, the grating had a deliberate chirp of 0.28 nm with decreasing wavelengths away from the gain medium, a reflectivity of 33%, and a grating length of 10 mm. The fiber lens had a hyperbolic shape to maximize coupling to the grating. The coupling efficiency of this type of lens can be as high as 98% [19]. With an HR coating on the rear and an AR coating on the output facet, the threshold of the device was measured to be 7 mA, operating single-frequency at fiber output powers of >15 mW. A side-mode suppression ratio (SMSR) of 56 dB was also demonstrated at a bias current of 250 mA(~25 mW output power). The linewidth was measured to be between 100 and 540 kHz (close to a mode hop), depending on the bias current.

An important application of the fiber Bragg grating is for stabilization of erbium amplifier pump lasers operating at 980 nm [20,21]. Since the pump absorption band is narrow, it is useful to maintain the pump wavelength accurately. It was found empirically that placing a 4% reflector reflection grating approximately 50–100 mm away from the AR-coated facet of a high-power pump-laser chip caused it to lock to the grating. Temperature variations of 50°C pulled the wavelength by ~0.2 nm, showing that the requirement for a thermoelectric cooler may not be necessary.

Such a long cavity (as with the one described earlier [12]) works under the regime of "coherence collapse" [22], where the coherence length of the diode modes is much shorter than the laser cavity length.

An alternative method of controlling the wavelength of the laser is to use the fiber grating at the rear facet of the chip [23]. The output coupler is a standard fiber pigtail. This device was fabricated in a package with all the in and out coupling with aspherical collimating lenses, as well as an isolator in the output path. The advantage of this scheme is the use of a highly reflective grating (>95%), potentially increasing the output power. The grating had a bandwidth of <0.4 nm, which was burnt-in at 350°C for 6 min. The fabrication technique is claimed to have a reproducibility of ±0.05 nm, allowing devices to be fabricated to ITU-T standards for dense WDM. With temperature control of the package, both the grating and the laser chip are maintained at the same temperature. Consequently, the stability of the wavelength was reported to be better than ±0.005 nm, with an output power stability within ±0.02 dB. This laser, as is common with well-designed FEGSLs had a measured linewidth of <30 kHz and a side-mode suppression ratio of >50 dB.

A combination of a reflective amplifier and a large spot laser has resulted in a robust laser, which may be operated over a wide temperature range without temperature control [24]. This type of laser has good wavelength stability as a function of temperature and therefore is ideally suited to applications in Access to a local area network, with the potential of being a low-cost source. Figure 8.3 shows a schematic of this laser. The gain medium is a semiconductor chip, which has a passive tapered waveguide to allow the mode to expand so that it has a mode-field close to that of a standard telecommunications fiber. Further, the waveguide is arranged to terminate at an angle to the output facet. The large mode field size

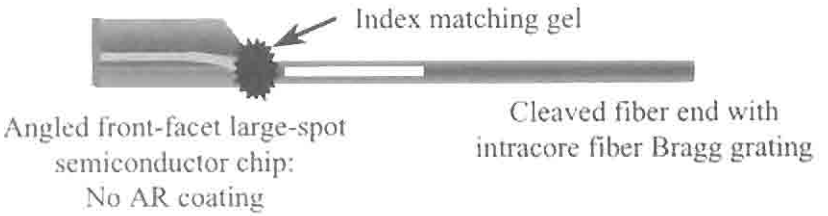


Figure 8.3: The large spot-angled facet, cleaved standard fiber FGSL [24].

allows good coupling to a cleaved standard fiber [24,25], which can be covered in index matching gel to reduce end reflections to a very low level. The angled facet ensures low back reflection, virtually eliminating the formation of a subcavity. No ripple due to intracavity reflections can be seen in the amplified spontaneous emission (ASE) spectrum. The positive effect of such a design is the lack of mode competition between subcavity modes as the current is ramped. A large-bandwidth (0.3-nm) fiber Bragg grating reflector allows the lasing mode to tune slightly in wavelength as the laser is modulated, with the virtual absence of mode hops.

The alignment is simplified with the help of a mini silicon-optical bench. A key on the bench allows easy positioning and soldering of the laser chip. A silicon micro-machined vee-groove aligned to the laser completes the passive alignment of the assembly. A glass sliver is then used to bond the fiber in place with epoxy. The gap between the laser and the fiber-end is then filled with gel. The package may then be completed by injection molding [25] or by hermetic sealing. A photograph of the packaged laser is shown in Figure 8.4.

8.2 Static and dynamic properties of FGLs

The light–current characteristics are shown in Fig. 8.5. The kink-free curve shows mode-hop-free operation as a function of bias current. The extremely low hysteresis in the wavelength of the laser as the current is altered, shows the potential of such a device. Typical of most FGLs is the weak temperature dependence of the lasing wavelength when the grating

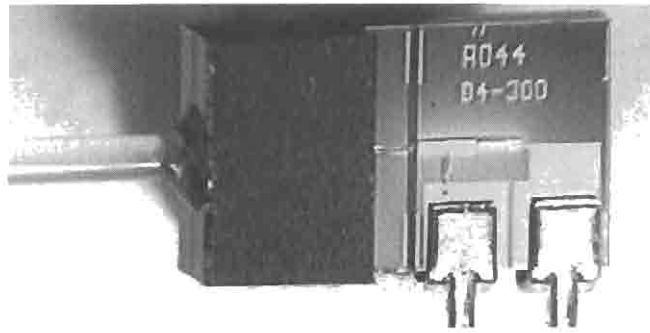


Figure 8.4: Photograph of packaged laser large spot laser FGL (photograph courtesy C. Ford, BT Laboratories).

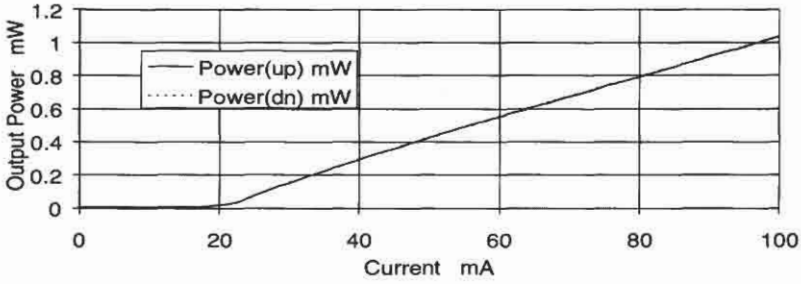


Figure 8.5: *L–I* characteristics (up and down) of large-spot angled facet laser at 20°C with index-matched gel between laser facet and cleaved fiber end. (Courtesy M. C. Brierley, BT Laboratories.)

is heated along with the laser. Mode hopping may be observed as the temperature is increased, as shown in Fig. 8.6. The cavity length determines the magnitude of the wavelength hop, and for this laser, it is ~0.16 nm. Note that the overall change in the lasing wavelength is approximately 0.4 nm for a 25°C change in temperature. With an unheated grating, the drift in the wavelength is made almost insignificant. The increased stability of a short-cavity semiconductor laser in an external long passive cavity has also been demonstrated [11].

With an AR-coated front facet reflectivity of 5×10^{-5} and a grating reflectivity of 28%, it has been shown that this type of laser may be

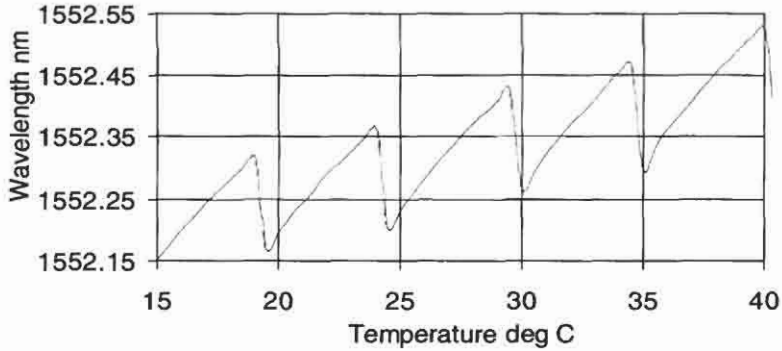


Figure 8.6: Wavelength vs temperature characteristics of the large mode-field FGL with index-gel. The grating is heated along with the laser chip. (Courtesy M. C. Brierley, BT Laboratories.)

ramped from threshold to 100 mA without a mode hop, and with a wavelength change of only 0.1 nm [24].

The static and dynamic chirp measurements of 500-μm-long AR-coated (reflectivity $\sim 1 \times 10^{-5}$) angled facet GaAsPInP buried-heterostructure amplifier chips [24] show that the static chirp of the dominant FGL mode is ~ -0.06 GHz/mA, while the dynamic chirp is reduced to 0.016 GHz/mA. The fiber Bragg grating had a reflectivity of 30% with a FWHM bandwidth of 0.3 nm. This data is shown in Figs. 8.7a and 8.7b. This laser has also been

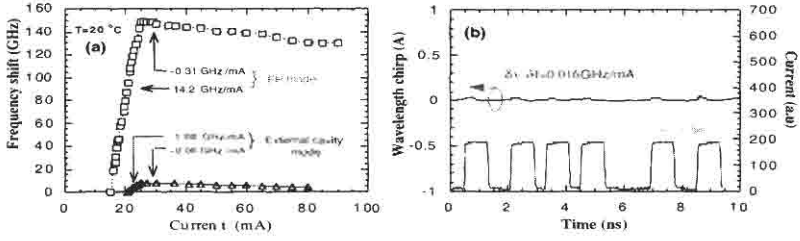


Figure 8.7: (a) Static chirp of external cavity and FP modes of the FGL; (b) shows the dynamic chirp under active modulation (from: Timofeev F. N., Bayvel P., Mikhailov V., Lavrova O. A., Wyatt R., Kashyap R., Robertson M. and Midwinter J. E., "2.5 Gbit/s directly modulated fibre grating laser for WDM networks", *Electron. Lett.*, **33**(16), 1406–1407, July, 1997. © IEE 1997, Ref. [30]).

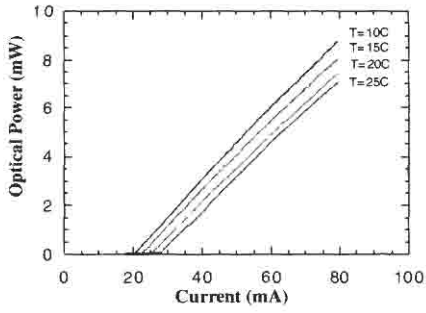


Figure 8.8: The kink-free light output characteristics of an angled-facet FGL with a 7-mm external cavity, as a function of temperature. Measured side-mode suppression ratio is -45 dB and RIN is -145 dB/Hz (from: Timofeev F. N., Bayvel P., Mikhailov V., Lavrova O. A., Wyatt R., Kashyap R., Robertson M. and Midwinter J. E., "2.5 Gbit/s directly modulated fibre grating laser for WDM network", *Electron. Lett.*, **33**(16), 1406–1407, July 1997. © IEE 1997, Ref. [30]).

shown to have extremely good thermal behavior, with the elimination of mode hops. The *L–I* characteristic at different temperatures shows kink-free operation over a wide temperature range, and the laser is therefore suitable for WDM applications. Figure 8.8 demonstrates the excellent coupling (high output power) and the smooth light output curves [30].

As a wavelength selector for a laser, the fiber Bragg grating offers a unique solution. The broad-gain bandwidth of semiconductor lasers combined with the quality of single-mode fiber connectors resulted in a "wavelength-uncommitted" laser [26]. A schematic of this device is shown in Fig. 8.9. The basic device consists of an AR-coated laser chip with a short fiber pigtail terminated in a fiber connector. Fiber Bragg gratings at various wavelengths, also packaged in fiber-FC-PC connectors, are then used to define the operating wavelength of the laser. A set of gratings allows a large

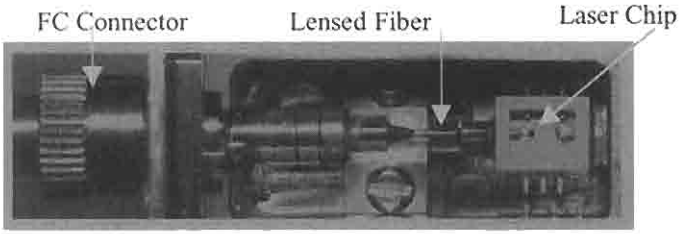


Figure 8.9: Wavelength-uncommitted laser [26].

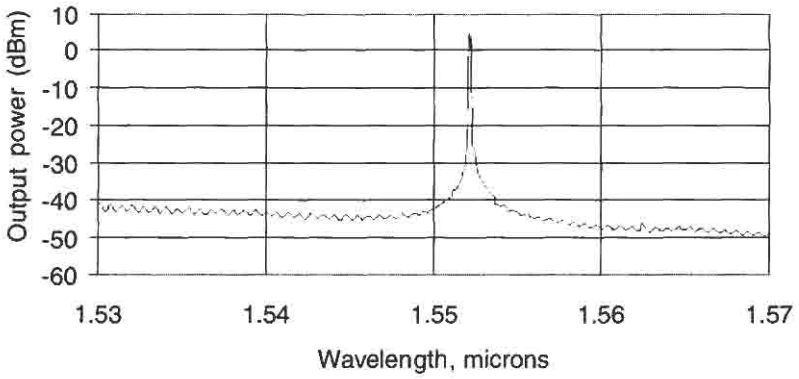


Figure 8.10: SMSR of ~50 dB for a fiber grating semiconductor laser with an output power of ~2 mW.

part of the gain band to be used. A semiconductor laser was shown to lase from 1480 to 1573 nm. The SMSR was measured to be ~50 dB for such a laser, at a power output of 1 mW in the fiber. Figure 8.10 shows the emission spectrum. This laser was shown to operate single-frequency at all wavelengths. However, the temperature has to be controlled carefully to prevent mode hopping and allow stable operation. A combination of the uncommitted laser concept and the large-spot laser should result in a cheap solution for wavelength selection.

Apart from applications that require the use of a modulation technique external to the laser, direct modulation of FGLs is desirable for low-cost devices. A large number of factors, such as electrical capacitance and inductance, cavity roundtrip, bandwidth of the external grating, and the interplay between the sub- and supercavity reflections, influence the dynamic behavior of FGLs. It has been shown that an external cavity laser with strong feedback can operate with high stability [3].

Provided the laser is operated within mode hops, the modulated performance has been shown to be excellent at transmission rates in excess of 2.5 Gb/sec [27–30]. Further, application of a FGL for millimetric-wave generation has been investigated [31]. In the latter demonstration, the modulation frequency injection locks two otherwise unstable lasing modes within the grating reflection spectrum to produce a high spectral purity RF beat signal at ~35 GHz.

With a short external cavity multi-quantum-well (MQW) FGL, modulation at >10 Gb/sec is possible for optical fiber transmission [32]. This design relies on the high-differential gain and low intrinsic chirp of a strained MQW, AR-coated front facet FP laser and the high-speed chip design using semi-insulating blocking layers. The linewidth of this laser was measured to be 40 kHz (~13 GHz roundtrip resonance; 8-mm external cavity), with −3 dB modulation bandwidth of ~15 GHz. The frequency response of the laser for different bias currents is shown in Fig. 8.11. The external cavity resonance is clearly visible as the current is increased to 100 mA. Measurements have shown that the chirp of this laser remains <10 MHz/mA compared with ~250 MHz/mA for a standard DFB laser. With a 2-mm-long external-cavity FGL, the frequency response is extended beyond 20 GHz [32].

8.2.1 Modeling of external cavity lasers

Figure 8.12 shows a schematic of a semiconductor laser coupled to an external cavity. Also shown are the parameters that need to be taken into account

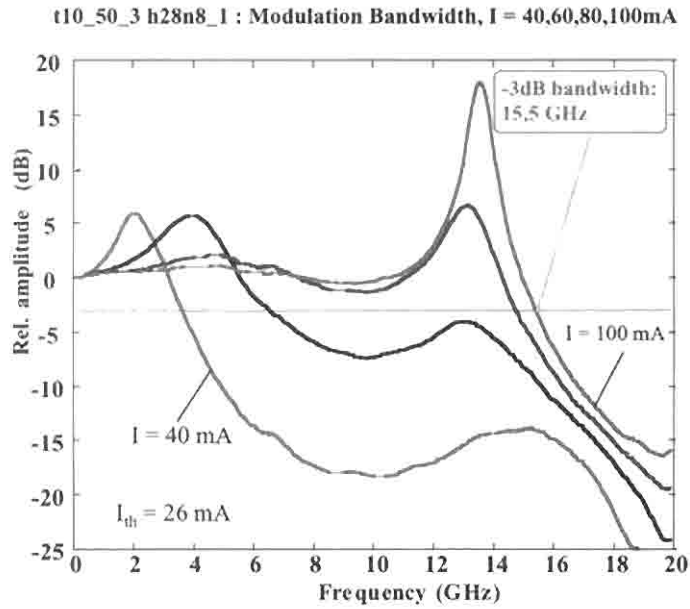


Figure 8.11: The frequency response of a FGL comprising a high-speed strained MQW and 8-mm-long external cavity (from: Paoletti P., Meliga M., Oliveti G., Puleo M., Rossi G., and Senepa L., "10 Gbit/s ultra low chirp 1.55 μm directly modulated hygrid fiber grating semiconductor laser source," in *Tech. Digest of ECOC'97*, pp. 107–110, 1997. © IEE 1997, Ref. [32]).

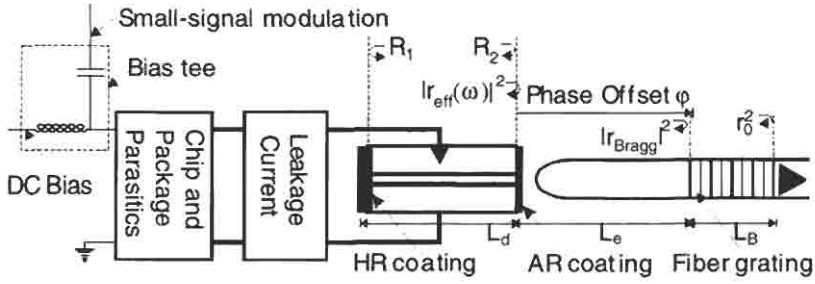


Figure 8.12: Schematic diagram modeling of the FGL. (AR: antireflective coating; HR: high reflective coating) (from: Premaratne M., Lowery A. J., Ahmed Z., and Novak D., "Modelling noise and modulation performance of fiber Bragg grating external cavity lasers," *IEEE J. Selected Topics in Quantum Electron.* **3**(2), 290–303, 1997. © IEEE 1997, Ref. [33]).

for modeling the laser: the reflectivities of the front and rear facets, the reflectivity and length of the grating, and the phase offset between the laser and the grating (passive fiber cavity), as well as the electrical contribution due to leakage, parasitics in the packaging, bias, and modulation signals.

Premaratne *et al.* [33] have presented a comprehensive rate-equation model for strong feedback taking account the many internal reflection of the composite cavity, based on the work of Park *et al.* [34], as well as the delayed fields from the reflections. Multiple reflections are accounted for by assuming that the field components are stationary [35]. Their analysis is therefore restricted to periodic and nonperiodic steady-state solutions. Transient response of FGLs has been investigated by Berger [36], while mode locking of the FGL to produce soliton like pulses has been modeled by Morton *et al.* [37,38].

The rate equations used to model the FGL are of the form [39,40]

$$\frac{d\boldsymbol{E}(t)}{dt} = \left(i\omega + \frac{1}{2}(G(N) - \alpha_{scatt}) + \frac{\ln(\rho)}{\tau_L}\right)\boldsymbol{E}(t), \tag{8.2.1}$$

where $G(N)$ is the spatially averaged gain at the average carrier density, N, resonant cavity, ω is the operating angular frequency with external feedback, α_{scatt} is the scattering loss, ω_r is the reference angular frequency of the field envelope, $\overline{E}(t)$,

$$\overline{E}(t) = \sqrt{I(t)}e^{i[\omega_r t + \varphi(t)]}, \tag{8.2.2}$$

$I(t)$ is the instantaneous intensity at time, t, and $\varphi(t)$ the instantaneous phase.

In Fig. 8.13 is shown the modeled steady-state *L–I* characteristics of a typical FGL with strong feedback and relatively large front-facet reflectivity of 0.04, and grating length of 8 mm. The choice of the initial phase condition at the interface determines the occurrence of the mode hop at around 30 mA, at either side of which the laser operates in a single longitudinal mode. The instability in this region is a result of the multimode nature of the long external cavity, predominantly due to the residual front-facet reflection.

Mode hopping can be eliminated by careful choice of operating temperature, as shown in Fig. 8.6, or by the reduction of the front-facet reflectivity. Interference effects due to delayed fields of the external cavity have been shown to be critical for predicting the stable performance of the FGL [33]. This effect of resonance-peak spectral splitting (RPSS) is shown in Fig. 8.14.

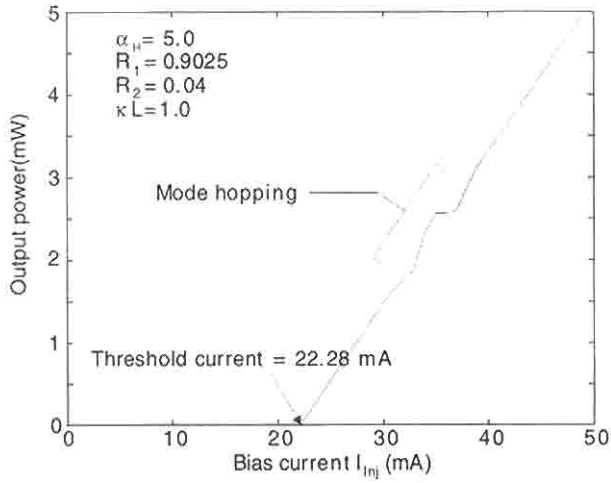


Figure 8.13: The *L–I* characteristics for an FGL laser with 4 GHz external cavity with a relatively large front-facet reflectivity (from: Premaratne M., Lowery A. J., Ahmed Z., and Novak D., "Modelling noise and modulation performance of fiber Bragg grating external cavity lasers," *IEEE J. Selected Topics in Quantum Electron.* **3**(2), 290–303, 1997. © IEEE 1997, Ref. [33]).

As the modulation frequency (close to the roundtrip frequency) is varied as a function of bias current, the output of the laser undergoes a series of peaks and dips. At a bias current of 37 mA, a steady single resonance peak is established, leading to stable operation. This situation is similar to the instabilities in the lasing characteristics of FGLs observed by Timofeev *et al.* [11] under modulation. Modeling shows the importance of the intracavity interference [33] in the vicinity of the mode-hopping regime. The alpha parameter strongly influences the RPSS, with low values of α and front-facet reflectivity favoring stable operation. The relative intensity noise (RIN) spectra also show the appearance of RPSS as α is increased [33].

8.2.2 General comments on FGLs

It appears that reduced-length laser diode chips and short external cavities favor single-mode, mode-hop-free operation [11]. Further, low facet-reflectivity, high-speed MQW designs, and strong feedback from the fiber grating promote good-quality modulation characteristics [3,24,32]. Vari-

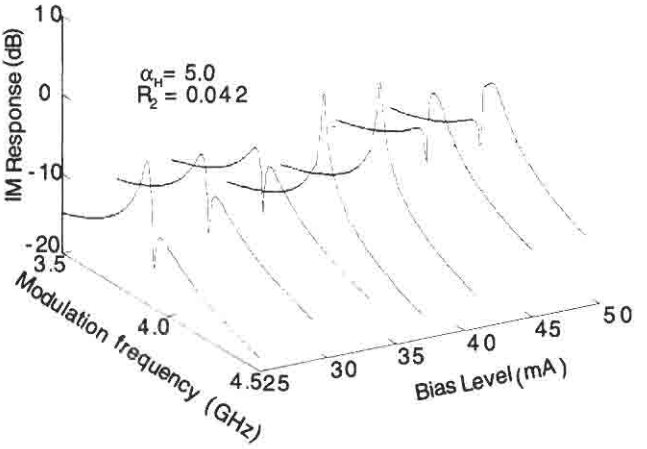


Figure 8.14: Change of RPSS vs bias current. Note the splitting position variation with bias current (4-GHz external cavity). The splitting may be reduced by a reduction in the front facet reflectivity (from: Premaratne M., Lowery A. J., Ahmed Z., and Novak D., "Modelling noise and modulation performance of fiber Bragg grating external cavity lasers," *IEEE J. Selected Topics in Quantum Electron.* **3**(2), 290–303, 1997. © IEEE 1997, Ref. [33]).

ous designs for the FGL show the alternatives available in reducing front-facet reflectivity by the use of a reflective amplifier [24], increasing coupling by the use of hyperbolic lenses formed on the ends of the fiber [19], chirped gratings to promote smooth *L–I* characteristics and allow stable mode-locking as well as the generation of soliton pulses [17,18], high-speed MQW designs for wide-bandwidth operation [32], plug-in gratings to allow selection of lasing wavelengths [26], and the use of coherence collapse for the injection locking of pump lasers [21]. The benefits of FGLs remain in the ability to define the lasing wavelength [26] and the low chirp [15,28,32] in improving the utilization of laser chips from manufactured wafers.

8.3 The fiber Bragg grating rare-earth-doped fiber laser

The concept of fiber lasers dates back to 1960. Snitzer [41] demonstrated a rod waveguide of smallish dimensions (0.5-mm diameter) doped with

ions of neodymium and dielectric end mirrors, which produced pulsed radiation when pumped with a flash lamp. Although it may be argued that the device was not a true *fiber* laser, the difference is merely in the detail, since it was a waveguide. With the advent of low-loss single-mode fibers [42] and the subsequent rare-earth-doped single-mode fibers [43], the early lasers still depended on external mirrors to choose the appropriate emission line. Although fibers enabled efficient end-pumping of these lasers, there were cases, as with Nd-doped fiber, in which the suppression of lasing of an adjacent competing line became difficult owing to the discrimination required of the resonator mirrors [44]. The problems were further compounded by the use of bulk reflectors or by the deposition of mirrors directly on the end faces of fibers [45]. In- and out-coupling had to be achieved through some form of mechanical alignment of mirrors, with high power densities at the mirror/fiber interface that usually needed a layer of index-matching oil for good optical contact. The first demonstration of the use of a narrowband in-line fiber reflector for a fiber laser used a 70% reflectivity grating etched into the core of a side-polished fiber [46]. While this scheme had the advantage of producing a narrow-bandwidth reflector (~0.8 nm FWHM), it had the disadvantage of being a device that needed considerable mechanical processing. The principle of tunability had already been demonstrated using a bulk diffraction grating as a frequency-selective reflector [47].

Thus, the photosensitive fiber Bragg grating, which was narrowband, low loss, and of adjustable bandwidth, was wholly suited to application in fiber lasers. The availability of compact high-power pump lasers at 1480 and 980 nm has made the fiber laser simple to fabricate. The high gain available in rare-earth-doped fibers allowed a nominal 0.5% reflection grating and a 100% bulk mirror with 30 m of erbium-doped fiber laser to produce 300 mW of power at 1537.5 nm when pumped with 600 mW of 980-nm pump [48] in the first photoinduced grating-based fiber laser. The ability to write Bragg gratings directly into rare-earth-doped fibers compatible with photosensitive fibers has resulted in a variety of successful demonstrations using either single or multiple gratings to form the resonator [49]. In the following section, generic examples of some of these lasers along with their properties will be examined.

Figure 8.15 shows a simple configuration of a single-cavity design of a fiber laser. The rare-earth-doped fiber has Bragg gratings as wavelength-selective mirrors. The laser is end-pumped via a WDM coupler normally through an optical isolator.

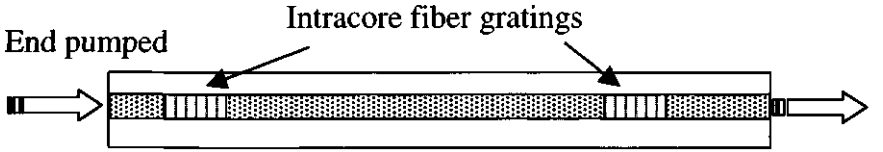


Figure 8.15: A schematic of the fiber Bragg grating rare-earth-doped fiber laser. The simple configuration encloses a piece of rare-earth-doped fiber between two Bragg matched gratings and is end-pumped.

The simple configuration allows a single-frequency laser [50,51] or twin laser configuration to be pumped in series with a single pump [52,53], or enables multiwavelength operation for sensor applications [54]. The transparency of the gratings to all other wavelengths allows closely spaced wavelengths to be emitted from one laser source, or the cascading of the laser with an amplifier section in a master oscillator power amplifier (MOPA) configuration [55]. A review of these lasers covers some of the general aspects [56]. Some of these lasers are considered in the following sections.

Spatial hole-burnt gratings may be used to stabilize semiconductor lasers. In the case, a piece of unpumped erbium fiber is used with a Bragg grating as the external cavity with an AR-coated semiconductor chip. The standing wave formed in the erbium doped fiber forms a population grating and line-narrows the laser. The 3-m-long cavity with a 1535-nm grating reflector was measured to have a linewidth of ~1 kHz [57].

High-power, double-clad Yb: doped fiber lasers with integral gratings in the cladding have achieved output powers in excess of 6.8 W in a single longitudinal mode [58]. At 1090 nm, 9-W fiber lasers are available that can be used as pumps for amplifiers and Raman oscillators (Section 8.7) [59].

8.4 Erbium-doped fiber lasers

The erbium ion in germanosilicate fiber has a three-level laser transition ($^4I_{13/2} \rightarrow {}^4I_{15/2}$), which may be modeled using the simplified three-level energy diagram of Digonnet [60]. A simple model for single-mode operation of an erbium fiber laser incorporating fiber gratings shows that the transient energy density per lasing mode is [61]

$$\frac{dE_n(z)}{dt} = \alpha I_n(z) - \gamma I_n(z), \tag{8.4.1}$$

where α and γ are the gain and loss for the lasing mode n. With negligible propagation losses, the loss is given as

$$\gamma = -\ln[R_o(\lambda)R_{HR}(\lambda)], \tag{8.4.2}$$

where $R_O(\lambda)$ and $R_{HR}(\lambda)$ are the reflectivity of the output coupling and high reflector gratings, respectively, at wavelength, λ.

The gain in terms of the steady-state ion population densities may be defined as

$$\alpha = (\sigma_e N_2 - \sigma_a N_1), \tag{8.4.3}$$

where the emission and absorption cross-sections are σ_e and σ_a, respectively.

The gain for two-moded lasers may be simplified in terms of the saturation intensity in the strong pump regime to

$$\alpha \approx \alpha_0 \left[1 - \frac{I_1(z)}{I_{sat}} - \frac{I_2(z)}{I_{sat}}\right], \tag{8.4.4}$$

where the saturation intensity is a function of the emission and absorption cross-sections, and α_0 is the small-signal unsaturated gain. The lasing photon intensities I_1 and I_2 are periodic within the cavity as a result of the formation of standing waves.

Using Eq. (8.4.4) in Eq. (8.4.1), the intensity of each steady-state mode is

$$I_{1,2} = \frac{I_{sat}}{3}\left(1 - \frac{\gamma_{1,2}}{\alpha_0}\right) - \frac{2}{3} I_{1,2}. \tag{8.4.5}$$

The slope efficiency at single-mode operation is then

$$\eta = \frac{\lambda_p}{3\lambda_1}\left[\frac{\sigma_p}{\sigma_a + \sigma_e}\right]\left[1 - \frac{\gamma_1}{\alpha_0}\right]\frac{A_1}{A_p}, \tag{8.4.6}$$

where σ_p is the ground-state absorption cross-section, A_1 is the lasing mode area, and A_p is the pump mode area. Substituting Eq. (8.4.5) into Eq. (8.4.1) and solving for the loss for the second mode results in the condition for stable single-mode operation,

$$\gamma_2 > \frac{\alpha_0}{3} + \frac{2\gamma_1}{3}. \tag{8.4.7}$$

Equation (8.4.7) states that the loss of the second mode must be greater than a third of the single pass gain plus the cavity roundtrip loss for the first mode. The reflectivity of the grating may be computed by the methods presented in Chapter 4 and used to determine the reflectivity for a given length of doped fiber with an unsaturated gain of α_0 per meter.

With the gratings written in highly doped erbium-doped fiber, the additional gain within the gratings must also be taken into account, since the effective reflectivity is increased [62]. The best region for single-mode operation is when the free-spectral range is twice the expected shift in the lasing frequency induced by perturbations and cavity length changes. This is greatly assisted by making the cavity as short as possible.

8.4.1 Single-frequency erbium-doped fiber lasers

Erbium-doped-fiber grating lasers (EDFGLs) offer a simple and elegant solution for wavelength selection, providing a very narrow linewidth as well as a high degree of wavelength stability. They are also compatible with optical fiber systems and can be easily integrated with other fiber components, such as WDM couplers and fiber isolators.

Tests performed on an externally modulated single-frequency EDFGL have confirmed its robust suitability for error-free high-speed application in transmission systems [50]. The laser is fabricated with 600 ppm GeO_2:Al_2O_3 doped silica fiber with a refractive index difference of 0.023 (core diameter of 2.6 μm) and cutoff at 880 nm. The tight confinement ensures high efficiency, and aluminum reduces the concentration-quenching effects that reduce the lifetime of the upper laser level, also leading to instabilities [63]. The gain of this fiber was reported to be ~10 dB/m, with an overall length of the laser of 4.4 cm, including gratings (98% O/P coupler and ~100% broadband high reflector), using the linear cavity design shown in Fig. 8.15. Pumped at 1480 nm, the laser is operated close to threshold to ensure single-mode operation and amplified in a MOPA configuration through an optical isolator. The packaged laser is sensitive to vibration that drives relaxation oscillation at a frequency of ~150 kHz. These oscillations can be actively controlled by using a feedback scheme to control the diode-pump laser and reduced to insignificant levels [50,64,65]. The error-free performance of several EDFGLs in transmission experiments at 2.5 and 5 Gb/sec been have reported [66,50,67], using external

Mach–Zehnder modulators. Upto 60 mW of single-frequency power has been achieved using a MOPA configuration [68].

Other configurations for single-frequency operation use long gratings with a bandwidth less than the cavity mode-spacing [69,70], and operation at 1 micron using Nd:doped fiber has been shown with intracore gratings [71].

Composite cavity lasers

There are several methods for achieving single- and multifrequency operation of EDFGLs. As outlined already, short lasers with narrowband reflectors are simple candidates; however, a composite cavity topology can enforce stable single-frequency operation by longitudinal mode control, adapted from semiconductor lasers [72–75]. The principle relies on a small additional feedback element in the form of a short Fabry–Perot, which modulates the gain spectrum of the main fiber laser cavity. Figure 8.16 shows the linear cavity configuration. The basic laser cavity gratings have reflectivities of 0.9 and 0.8 with a weaker reflection of 0.1 as the external reflector. The gain of the composite cavity is modulated, increasing the discrimination between the modes. Since the lasing mode is influenced by the composite cavity, a single mode tunes with temperature changes but does not exhibit mode hops [53]. The 10-mm-long high erbium dopant concentration fiber (120 dB/m absorption at 1530 nm) is spliced to fiber gratings, forming a composite cavity ~7 cm long; 980-nm pumping with a Ti:sapphire laser showed a threshold of 50 mW. The linewidth of this laser is ~40 kHz using conventional heterodyne techniques. The gain

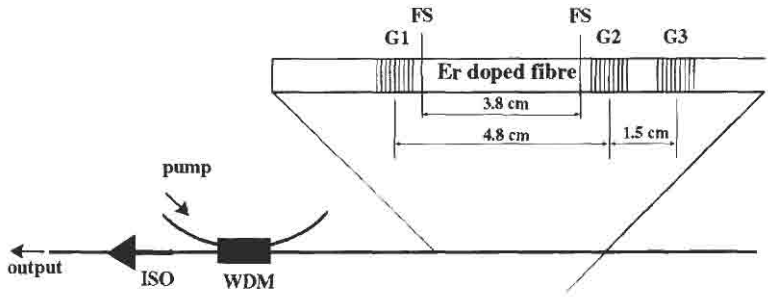


Figure 8.16: A schematic of the composite cavity single-frequency EDFGL [53].

bandwidth of such a laser with and without the extra etalon is shown in Fig. 8.17. With the external etalon, the gain is modulated at a frequency separation determined by the spatial separation and reflectivities of the gratings. The simulation in Fig. 8.17 shows the composite reflection spectrum of the two gratings without the additional feedback (dashed curve) and with feedback (solid curve). In this laser, the period of the frequency separation is 28 GHz without feedback and ~7 GHz with the etalon approximately half the mode spacing of the composite laser. The use of a very short gain region with respect to the cavity length (a factor of 3–4) eliminates the relaxation oscillation observed in other cavity designs [50] using erbium fiber.

Composite fiber gratings with ring or loop mirror cavities [76] are other possible configurations, and for single frequency operation with intra-cavity frequency selector [77]. An example of this cavity is shown in Fig. 8.18 in a loop mirror arrangement. In this cavity, the loop mirror is a broadband mirror, while the external fiber Bragg grating is a band-selecting element. The isolators inside the loop-mirror ensure unidirectional operation, while the incorporation of an ultranarrow band-pass

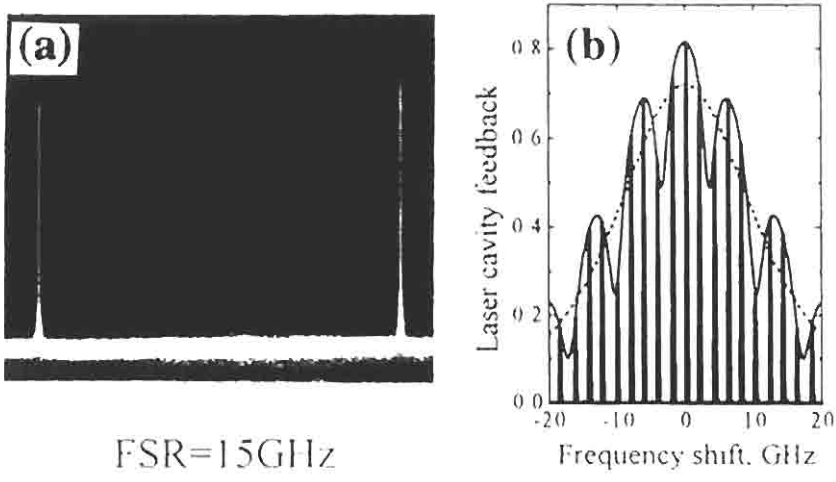


Figure 8.17: The reflectivity and mode selection spectra of the coupled-cavity EDFGL. Laser with feedback (solid line), and laser without feedback (dashed line) (from: Chernikov S. V., Taylor J. R., and Kashyap R., "Coupled-cavity erbium fiber lasers incorporating fiber grating reflectors", *Opt Lett* **18**(23), 2023 (1993). (after Ref. [53])).

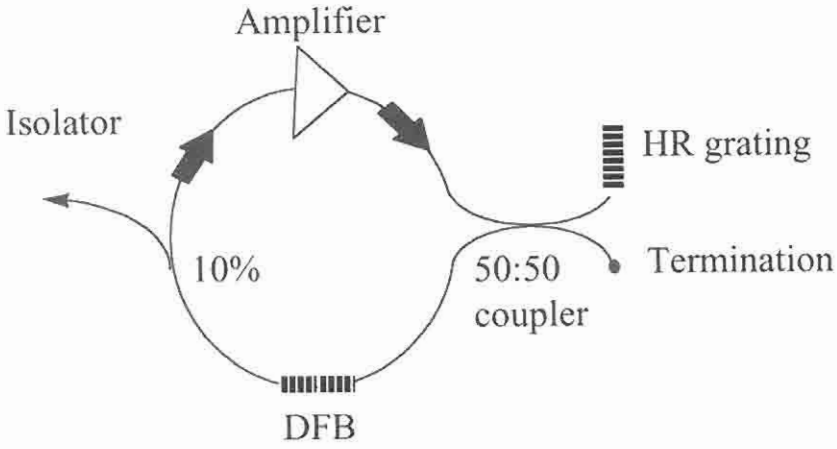


Figure 8.18: The loop mirror cavity for single-mode operation, incorporating a DFB band-pass filter and an erbium-doped fiber amplifier (after Ref. [77]).

DFB fiber Bragg grating (see Chapter 6), also inside the loop, enforces single-frequency operation. The laser may be tuned by applying compressive or extensive strain on the intracavity DFB grating or, in the absence of the DFB grating, the external grating. Single-frequency operation of such a laser with a 0.075-nm band-pass DFB grating shows a linewidth of ~2 kHz, with side-mode suppression of 50 dB. However, the long cavity with a mode spacing of 11.4 MHz mode hops and requires the use of stabilizing elements [77].

Replacing the DFB band-pass intra-cavity filter by an acousto-optic tunable filter (AOTF) may extend the principle of this type of a laser. Ramping the AOTF sweeps the output frequency of the laser with <0.1-nm linewidth [78].

To improve the strength of the grating, a specially deposited photosensitive ring cladding can be fabricated with a rare-earth-doped core. This scheme allows the core to have a high dopant concentration, while preserving the fiber's photosensitivity and allowing short, high-strength grating to be inscribed for laser fabrication [79,80].

8.5 The distributed feedback fiber laser

The principle of the distributed-feedback (DFB) structure, generally applied to semiconductor lasers [81], is easily translated to doped fiber

lasers. Figure 8.19 shows a schematic of the laser, which is identical to a Fabry–Perot laser, except that the two gratings are separated by only a quarter-wavelength (see Chapter 6). The phase shift generates a gap in the reflection spectrum, allowing narrow single-frequency operation.

With the possibility of writing gratings directly into erbium-doped fibers (see Chapter 2), DFB lasers may be fabricated with ease, especially since long gratings (~100 mm) require modest refractive index modulations to produce a high reflectivity. The first reported DFB laser operated at 1 micron and was fabricated in ytterbium-doped fiber [82]. It has been successfully demonstrated in erbium-doped fibers for 1500-nm operation [83,84] and extended by cascading five DFB lasers separated in wavelengths by ~1 nm each, pumped by a single 1489-nm diode laser [85].

Simple modeling of a DFB laser may be achieved by including a gain (complex term) in κ_{dc} in [Eqs. (4.3.5) and (4.3.6)], so that $\Delta\beta$ is modified by $i\gamma$, where γ is the gain per meter. Numerical simulation of the transfer function in Chapter 4 [Eq. (4.8.22)] of the DFB is shown in Fig. 8.20 as a function of increasing gain. As the gain increases, the side modes of the DFB structure begin to lase.

There are two possibilities for inducing a phase shift in the grating: one which is localized, or by distributing the phase shift along the length, as discussed in Chapter 6. The model takes account of the variation in the gain as a result of pump depletion. It has been shown for a 5-cm-long DFB laser that positioning the discrete π phase-shift away from the center of the laser, at $\sim 0.6L_{DFB}$, increases the output power by as much as 60%. For a phase shift distributed over 1 cm of the same laser, the optimum value acquires a slightly larger value of 1.3π radians [86].

The position of the phase shift changes as a direct result of spatial hole burning, since the intensity is highest at the center of the laser for a symmetrically positioned phase shift. The distributed phase-shift laser is as efficient as the discrete off-center phase-shifted laser.



Figure 8.19: The EDFGL distributed feedback laser (EDFGL-DFB). The phase shift of $\pi/2$ forms a band pass in transmission.

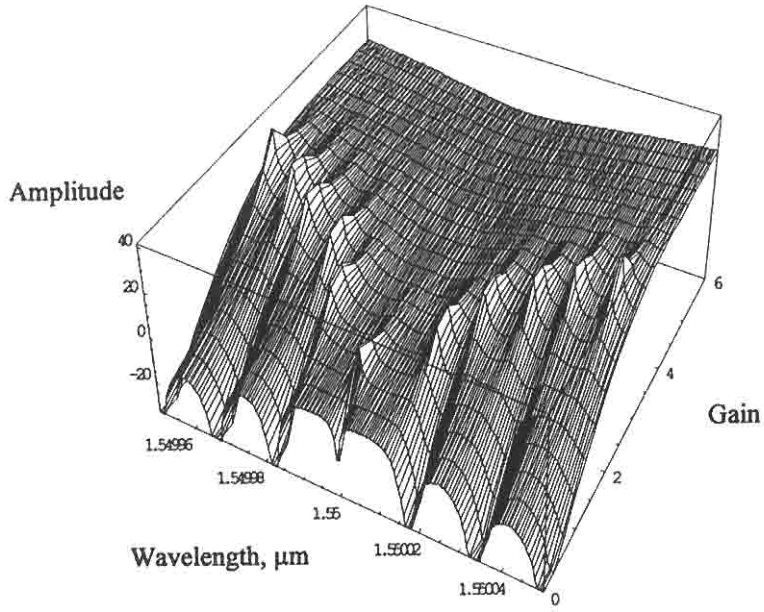


Figure 8.20: The transmission spectrum of a 100-mm-long DFB laser as a function of the gain.

8.5.1 Multifrequency sources

Dual-frequency and multifrequency sources can be built by combining techniques presented in the preceding sections. A novel and particularly simple arrangement is the four-grating coupled cavity arrangement based on the single-frequency laser shown in Fig. 8.16. By adding an extra grating matched to the external grating in Fig. 8.16, a dual-frequency laser is formed. In order to ensure the coupling between the cavities, the grating bandwidths are chosen to overlap slightly. This configuration produces a robust laser that performs as a *single* entity, and a schematic is shown in Fig. 8.21. The emission spectra consist of two single-frequency lasing modes at defined by the grating pairs, and tune without mode hops. However, the difference frequency tunes with temperature, strain, or pump power (thermally induced). The coupled cavity reported by Chernikov *et al.* [52] operated at a difference frequency of 59.1 GHz centered around 1545 nm, with a long-term average linewidth of ~16 kHz and a stability of the dual frequency of ~3 MHz.

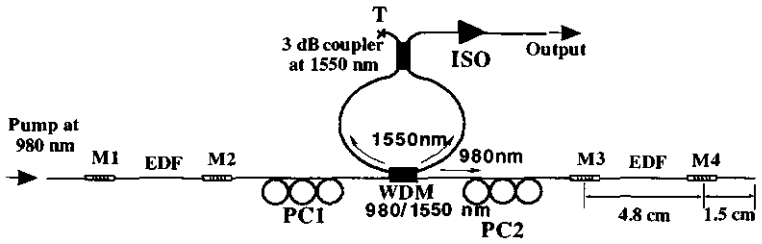


Figure 8.21: The coupled-cavity dual-frequency source (from: Chernikov S. V., Kashyap R., McKee P. E., and Taylor J. R., "Dual frequency all fiber grating laser source," *Electron. Lett.* **29**(12), 1089, 1993. © IEEE 1993, Ref. [52]).

Multifrequency operation in ring lasers has been reported with the use of a grating with a multiple wavelength reflection spectrum. Up to 8 wavelengths have been shown to lase simultaneously. While single-frequency operation (~10 kHz linewidth) has been demonstrated, in such long lasers, mode hopping is common, and special attention must be paid to stabilize the operation [87].

8.5.2 Tunable single-frequency sources

The gain bandwidth of doped fibers is several tens of nanometers. Tunability is possible with fiber Bragg gratings by strain or temperature tuning (see Chapter 3). Ball and Morey [88] stretch-tuned a pair of Bragg gratings of a 100-mm-long erbium fiber laser and showed 9 GHz mode-hop-free operation. Since the gratings and the fiber length tune together, the laser remains stable. Compression tuning can extend the tuning range, and a tuning range of 32 nm has been reported for a short EDFGL (3 cm) in a MOPA configuration. Continuous single-frequency tuning was observed with the laser producing 3 mW of output. A feedback loop is necessary to stabilize the operation of the laser to reduce relaxation oscillations [89]. Compression tuning of a Yb/Er laser using a mirror and Bragg grating configuration has shown sub milliwatt thresholds and both strain and compression tuning ranges of up to 25 nm [90].

8.6 Bragg grating based pulsed sources

We have seen that the FGL can be used as a pulsed source for optical fiber transmission, either directly modulated or mode-locked [15,17,

18,24,27,32]. We have also seen that the EDFGL is an excellent candidate as a source [50]. There are several alternative methods of generating short pulses in conjunction with gratings, for example, semiconductor laser pulse compression in a chirped grating [91,92], using the dual-frequency source and adiabatic soliton pulse compression [93] and linear actively mode-locked fiber laser [94].

Pulse compression of gain-switched DFB and FP lasers [95] is possible using a dispersive delay line, since the emitted pulse is chirped in time and frequency. If the dispersion of the delay line is opposite to that of the pulse, it may be compressed. Chirped gratings (see Chapter 7) are ideal candidates, since they are compact and the dispersion can be tailored for a particular application. The experimental setup is shown in Fig. 8.22. A pulse train at 500 MHz from a gain-switched DFB laser is reflected from a chirped grating and the recovered pulse is compressed. Figure 8.23 shows autocorrelation

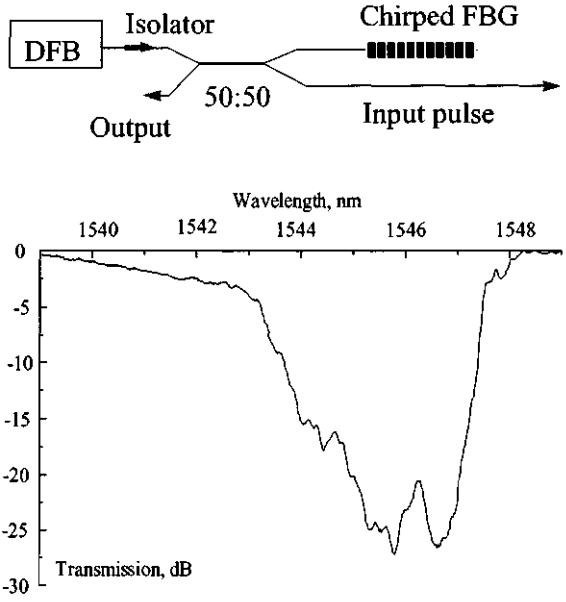
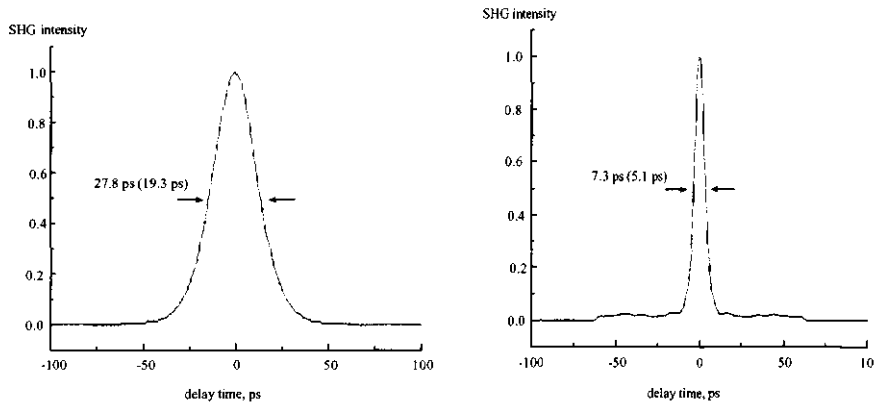


Figure 8.22: Experimental setup for pulse compression and transmission spectrum of the chirped fiber grating (from Gunning P., Kashyap R., Siddiqui A. S., and Smith K., "Picosecond pulse generation of <5ps from gain-switched DFB semiconductor laser diode using a linearly ste-chirped grating," *Electron. Lett.* **31**(13), 1066–1067, 1995. © IEEE 1995, Ref. [91]).



(a) (b)

Figure 8.23: Input pulse from the gain-switched DFB (a) and reflected pulse form the chirped fiber Bragg grating (from Gunning P., Kashyap R., Siddiqui A. S., and Smith K., "Picosecond pulse generation of <5ps from gain-switched DFB semiconductor laser diode using a linearly ste-chirped grating," *Electron. Lett.* **31**(13), 1066–1067, 1995. © IEEE 1995, Ref. [91]).

traces of the input and reflected pulse from the grating. The gain-switched pulse has chirped a bandwidth of ~1.5 nm, and the 6-mm-long grating slightly filters the spectrum while recompressing the pulse. A small residual pedestal is due to the uncompensated part of the spectrum. The technique is simple and requires a minimum of control.

The second scheme for compressing a sine wave into pulses is based on a combination of adiabatic perturbation and average soliton regimes of propagation. During an adiabatic perturbation, there is a balance between the dispersive and nonlinear contribution by a change in the soliton duration [96]. In the average soliton regime, there is balance between the periodically varying dispersion and nonlinearity [97]. The use of this scheme allows the slow transformation of a modulated input signal into a soliton. An amplified optical sine wave is launched into a long length of fiber. It periodically undergoes self-phase modulation in a zero-dispersion section of a fiber, increasing the spectral content and linear dispersion in a high-dispersion part of the transmission line. By selecting the appropriate combination of dispersion and nonlinearity, the average dispersion of the link is reduced approximately exponentially. The reducing average dispersion continually compresses the optical sine wave into soliton pulses.

A similar scheme for generating solitons was reported using dispersion decreasing fiber [98], based on the earlier predictions [99]. The source used for pulse generation is the dual-frequency EDFGL source shown in Fig. 8.21 [100]. The narrow line-widths of this source produce an optical beat signal. To eliminate stimulated Brillioun scattering, different germania concentration fibers are used in the 20-section comblike dispersion profiled fiber (CDPF), with a total length of ~7.5 km. A beat signal at an amplified power of 190 mW and frequency of 59.1 GHz are converted into pedestal-free sech^2-shaped pulses with a FWHM of 2.2 psec, at a wavelength of 1545 nm [93]. Several other configurations based on the beat-frequency generation may be found in Ref. [101].

Mode-locking of fiber lasers has been investigated in a variety of "figure-eight" configurations [102] using fiber gratings to generate multiwavelength pulses. Actively mode-locked dark-pulse generation from a praseodymium-doped fiber laser with a chirped grating has also been reported [103].

8.7 Fiber grating resonant Raman amplifiers

Raman scattering is a process in which a small fraction of the incident light is scattered by the vibrational modes within a material to generate a Stokes photon, downshifted in frequency. Stimulated Raman scattering (SRS) is a process by which the Stokes photon interacts with the pump photon to generate another Stokes photon and is described by the imaginary part of the nonlinear susceptibility, $\chi^{(3)}(-\omega_s;\omega_p,-\omega_p,\omega_s)$. The Stokes field grows exponentially with the length of the medium. Since its discovery [104], SRS has been a topic of considerable research [105]. SRS can be a very efficient process, strongly depleting the pump power. With the advent of optical fibers, the observation of SRS has become very easy because of the high power densities in the core, low optical loss, and long interaction lengths. The Raman gain, which depends on the scattering cross-section, has been measured in silica optical fibers [106]; the bandwidth, because of the amorphous nature of the glass, is extremely large, extending over some 40 THz with a peak at 13 THz from the pump wavelength. Below the threshold for SRS, a signal photon, downshifted from the pump frequency, experiences gain if it lies within the gain bandwidth. This is the principle of Raman amplification [107].

If a fiber is placed between mirrors and pumped, the Stokes field sees a roundtrip gain of

$$G = e^{2g_R I_0 L_{eff}}, \tag{8.7.1}$$

where g_R is the Raman gain coefficient, I_0 is the intensity of the pump, L_{eff} is the effective length of the fiber $\sim 1/\alpha_{pump}$ (the fiber loss at the pump wavelength), and the factor of 2 is for the double pass. The pump intensity at which the Stokes field overcomes the cavity losses for a given set of mirror reflectivities is called the threshold for oscillation. For 10 m of fiber, a CW threshold can be reduced to ~1 W [108,109]. As the pump power is increased, the Stokes field S_1 increases until the threshold for the second-order Stokes S_2 is reached, at which point energy is transferred to S_2. At this point, a signal at the third Stokes frequency will experience gain, and so on. This is also the principle of the resonant Raman amplifier. This type of a multi-Stokes oscillator has been demonstrated by Stolen *et al.* [110,111], who generated five Stokes orders of independently tunable radiation.

Perhaps one of the most elegant components that is the direct result of the high transparency of Bragg gratings outside the band stop is the Raman fiber grating laser, the RFGL. This laser has opened many opportunities in communications, by allowing amplification in *any* part of the communication spectrum by appropriate choice of pump lasers and fiber Bragg gratings.

The general cavity configuration for a resonant Raman laser [112] is shown in Fig. 8.24.

This laser has been shown to produce 1.5 W at 1485 nm when pumped by a diode-pumped Yb^{+3} double-clad laser. The Yb^{+3} pump at 1117 nm

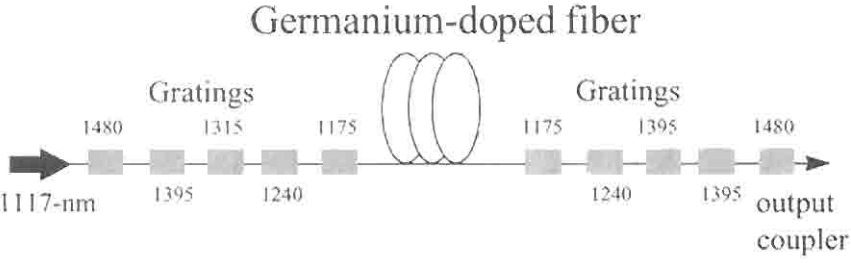


Figure 8.24: Cascaded fiber grating resonant Raman 1480-nm pump laser for pumping erbium amplifiers [113].

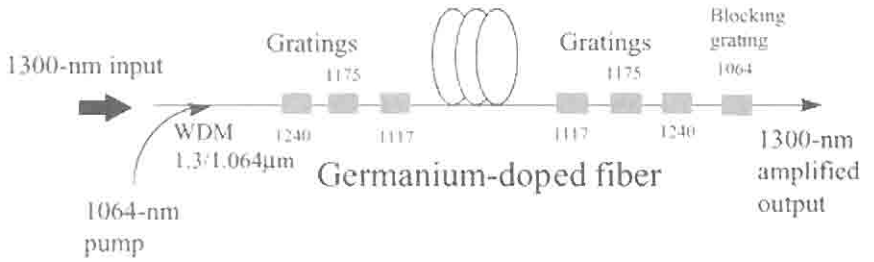


Figure 8.25: Schematic of a 1300-nm cascaded fiber grating resonant Raman amplifier [115].

produces in excess of 6 W CW. The five stages Stokes of conversion is remarkable, showing ultralow loss of <0.2 dB per grating.

For 1300-nm amplifiers, two configurations can be used. The linear cavity shown in Fig. 8.25 uses WDM couplers and a set of gratings to allow gain in the 1300 nm window when pumped by a 1.064 nm source. The gain is available at the fourth Stokes wavelength. These amplifiers have gains as high as 40 dB with saturated output powers of 24 dBm. With higher germania concentration (higher Raman gain) the pump power can be lowered to 300 mW while providing a gain of 25 dB [114].

The theoretical noise figure for Raman amplifiers is 3 dB [116], while the achieved figures are around 4.4 dB at 40 dB gain in a ring configuration [117,118].

The advantage of using bidirectional pumping as in a ring cavity is reduced cross-talk and polarization sensitivity.

These amplifiers are increasing in importance as the requirement for the optical bandwidth increases. In regions of the communications window in which amplification is difficult, e.g., 1350–1500 nm, *cascaded* fiber grating resonant amplifiers are likely to provide unique solutions.

8.8 Gain-flattening and clamping in fiber amplifiers

Rare-earth-doped optical fiber amplifiers are important components in transmission systems. The transmission bit-rate × distance product is almost limitless in laboratory-based demonstrations [119]. This is primarily due to the "zero-transmission loss" through periodic amplification as

well as the management of dispersion. The fiber amplifier has enabled undersea transmission over thousands of kilometers. With the increasing demand for bandwidth, wavelength division multiplexing (WDM) of optical channels is seen to be a viable solution for increasing transmission capacity at a given transmission rate, in point-to-point routes [120].

The important issues in amplified transmission systems for WDM applications are the available gain, the gain uniformity across the bandwidth of an amplifier, the robustness to transient switching of WDM channels in single and cascaded amplifier chains, and the overall noise figure. The gain spectrum and upper-state lifetimes of an erbium-doped fiber amplifier vary as a function of the core dopants. High-germanium erbium-doped fibers have a highly nonuniform gain with a bandwidth of ~35 nm from 1530 to 1565 nm, peaking at approximately 1535 nm. The use of aluminum reduces the nonuniformity, making the gain spectrum flatter, while ytterbium as a codopant with erbium allows an efficient transfer of energy from the available high-power diode pumps at 980 nm (a wavelength at which erbium suffers from excited-state absorption, reducing efficiency) to the required transition in the 1550-nm wavelength region for amplification. The latter shifts the gain peak to >1540 nm, while narrowing the gain bandwidth. Along with the nonuniformity in the gain, the doped fiber amplifier is homogeneously broadened. While allowing amplification across the wide gain bandwidth, the gain available at any wavelength is dependent on the simultaneous presence or absence of other wavelength channels; thus, gain may be depleted from a saturating signal from an existing channel as another channel is switched on. As the gain in a single amplifier fluctuates, the problem is exacerbated with a chain of cascaded amplifiers, leading to severe cross-talk. Nonuniform gain across the bandwidth of the amplifier produces a wavelength-dependent low-frequency cross-talk penalty. Apart from the signal degradation, severe damage to components is a possibility because spiking with intermittent interruption and resumption of transmission. The inversion and thus the gain is also pump-power dependent, leading to gain changes as the pump source ages. For analog transmission systems the problem is worse, because the local gain slope leads to harmonic distortion, degrading the received signal. Schemes have been developed to stabilize the gain of fiber amplifiers as well as flatten the gain variation over a wide bandwidth. Fiber gratings offer simple solutions to solve both these problems. In the following sections, we look at a specific example of gain

flattening and gain stabilization and a combination of the two, using fiber gratings.

8.8.1 Amplifier gain equalization with fiber gratings

In Chapter 4 the properties of side-tap gratings (STG) and long-period gratings (LPG) were described. Both types of gratings may be used as narrowband, wavelength-specific, loss-inducing components. In particular, the STG, which is a tilted Bragg grating, couples a narrowband at the short-wavelength side of the Bragg reflection wavelength to a continuum of the radiation field in the case of the unbounded cladding. This requires matching the cladding with an appropriate oil/polymer to destroy the well-defined boundary. For an appropriate blaze angle, which also minimizes Bragg reflection into the guided mode, the radiated light has an angular and spectral bandwidth. At this blaze angle, the period of the grating determines the wavelength of peak loss. Adjustment of the grating period at the same tilt angle enables the loss to be placed at any position within the gain spectrum of the amplifier. It should be noted that coupling to the radiation field for the first-order grating interaction is restricted to a *local* loss spectrum, close to the Bragg reflection wavelength, and hence a combination of several such spectra allows the fabrication of complex spectral loss features. By appropriate choice of filters, the filter loss may be matched to the inverse of the gain variation in the erbium amplifier to flatten the gain spectrum. Both single [121] and multiple [122] STGs have been used to tailor the gain spectrum of erbium amplifiers. In the first instance, a single, 4-dB peak-loss, 10-nm bandwidth (full-width) grating was placed at the 1533-nm peak of the erbium amplifier, eliminating the gain variation. By appropriate choice of the grating period (with the use of a phase mask) the peak loss is moved anywhere within the gain bandwidth. The inversion and therefore the gain shape is dependent on the pump power. The filter is thus appropriate for a given inversion (gain).

Figure 8.26 shows eight such loss spectra with approximately identical shapes, but with different peak-loss wavelengths and insertion loss. Each filter is ~8 mm long with an external blaze angle of ~8°, chosen to minimize back reflection, written in a boron–germanium codoped fiber with a core diameter of ~12 microns (see Chapter 3).

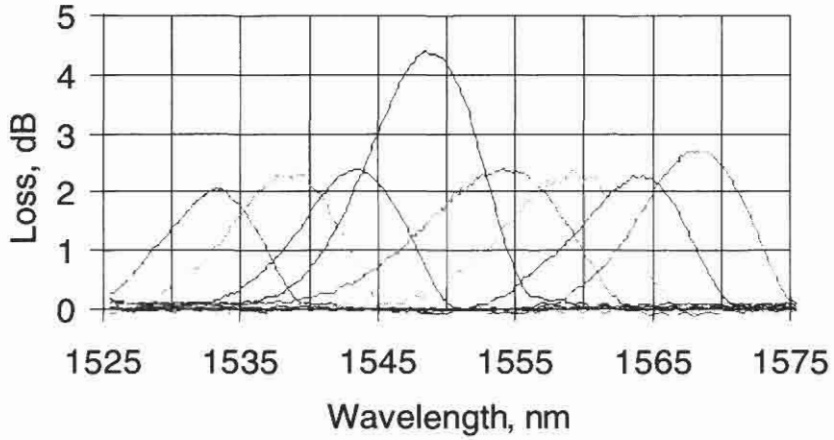


Figure 8.26: Radiation loss spectrum of eight STG filters written at an external blaze angle of 8° in a fiber with a core diameter of ~12 microns [122].

The use of multiple STG filters allows tailoring complex gain spectra with a greater degree of accuracy. The peak deviation over 3 dB from a fixed gain of 13.7 dB across the bandwidth of the amplifier is conveniently reduced to ±0.3 dB by the use of in-line STGs [122] and is shown in Fig. 8.27. The required loss spectrum is deconvolved into a number of contributions from individual gratings, prior to fabrication of the filter.

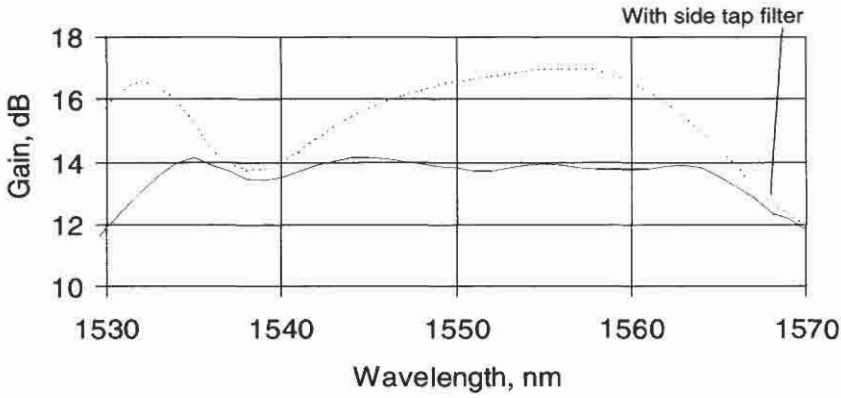


Figure 8.27: The ASE spectrum of a saturated erbium amplifier without and with a composite STG gain equalizing filter [122].

With this information, the filter is fabricated with the amplifier at its operating inversion level, allowing live gain tailoring. In this instance up to nine individual STGs were written to match the variation in the gain. Each grating can be ~1 mm long, making the entire gain equalization filter to be less than 10 mm. Such a filter may be written using a single phase mask appropriately designed to give the desired loss at each wavelength, by scaling the length of each grating or with an appropriate amplitude shading [123]. A distinct advantage of the STG is that the uncompensated temperature sensitivity of the loss spectrum is similar to that for Bragg grating, making the filter intrinsically stable. With temperature compensation as with Bragg gratings, the variation in the loss spectrum may be eliminated altogether over the required operating temperature range.

The tilt angle for the STG is chosen to minimize back-reflection into the guided mode (see Chapter 4). The transmission and reflection spectra of two STGs with peak-loss wavelengths separated by ~10 nm are shown in Fig. 8.28. The combined transmission loss of the two gratings it ~12 dB. The first grating is written at a blaze angle close to that required for a minimum reflection, while the second is written at a larger angle to increase the bandwidth of the composite filter. Each grating has a loss of approximately 6 dB. The first STG, which peaks at the shorter wavelength, has a reflectivity of −35 dB, while the unoptimized longer wavelength loss STG shows an increased reflection of ~21 dB. Typically, the gain variation in the amplifier spectrum requires each STG to have a

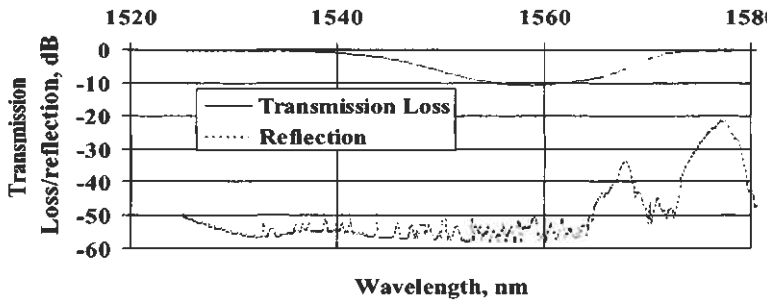


Figure 8.28: The transmission and reflection spectra of two STGs written in the same fiber. The 6-dB peak-loss STG 1 at the shorter wavelength has a reflection of −35 dB. The second unoptimized STG at a larger tilt angle has a higher reflection of −21 dB.

peak loss of less than 3 dB, resulting in a maximum back-reflection of <-40 dB.

Thus, a concatenation of STGs may be used effectively to flatten the gain of an optical amplifier, with low back-reflection. The design of the fiber to alter the bandwidth of the filters has been discussed in Chapter 4. This approach allows finer structures in the gain spectra to be matched more closely [124].

The application of LPGs for tailoring the gain of optical amplifiers has also attracted interest. The main feature of the LPG is the coupling of the guided mode to a forward-propagating *cladding* mode, one of which is selected from a large number, to induce the desired loss at the appropriate wavelength within the gain spectrum. It should be remembered that several mode interactions, widely separated in wavelength, occur in tandem for a given grating period. As such, LPGs have been used to equalize the gain of erbium amplifiers [125,126] and as ASE-suppressing filters. The technique used for forming the gain-equalizing filter is identical to that for the STG and has been already described [122]. There are major differences between the STG and the LPG. The latter exhibits more than a single loss peak separated by ~30–60 nm, depending on the type of fiber used for the filter. Written in standard telecommunications fiber, the temperature sensitivity of the LPG is roughly 4–5 times that of the STG. However, it has a low back-reflection into the guided mode of ~ -80 dB.

Unless the LPG is fabricated in special temperature-stabilized fiber, the amplifier gain equalization remains temperature sensitive, leading to gain tilt. Finally, the wavelength of the peak loss is a function of the refractive index of the material surrounding the cladding. With an appropriate low-index polymer coating, the cladding mode resonance is made insensitive to the surrounding material. The LPG has been used extensively in gain equalization of amplifiers and remains an important component.

Another method of equalizing the gain of an erbium amplifier is by the use of two or more apodized reflection gratings in series with an optical isolator. The resultant spectrum is shown in Fig. 8.29. Gain equalization to approximately ± 0.5 dB may be achieved with this simple arrangement.

Since gain flatness of the optical amplifier with filters is dependent on the level of inversion, it becomes particularly attractive to combine the filter with all-optical gain control, which is considered in the next section.

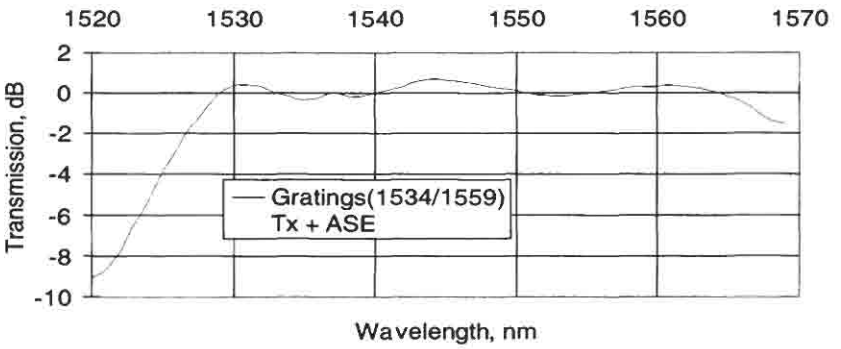


Figure 8.29: The simulated gain spectrum of an erbium amplifier equalized by two reflection gratings of lengths 0.2 and 0.061 mm centered at 1534 and 1559 nm. (The refractive index modulations for the two gratings are 3.5×10^{-3} and 1.06×10^{-3}).

8.8.2 Optical gain control by gain clamping

There are a variety of ways of stabilizing the gain of erbium-doped fiber amplifiers. In particular, sampling the state of the amplifier and deriving some sort of feedback, for example, signal levels [127], ASE [128], or a dedicated probe [129], to adjust the amplifier's pump power, or sacrificial injected signals have also been proposed [130,131]. These in turn limit in the frequency response by introducing electrical delays in the feedback loop. A simpler and more elegant all-optical approach to gain stabilization of an erbium doped fiber amplifier was first reported by Zirngibl [132], using lasing action in a ring cavity configuration. In a homogeneously broadened system, the inversion and therefore the gain remains constant irrespective of input signal level or the number of input channels. The amplifier remains robust against transients and to the switching of channels, so long as the amplifier continues to lase at some wavelength within the amplification window. The gain is maintained at the expense of the flux in the lasing mode. This "gain-clamped" amplifier is especially useful for cascading and in dynamically changing optical networks. The amplifier design is greatly simplified by the use of a linear cavity made with narrowband, highly reflecting Bragg gratings [133]. Delevaque *et al.* demonstrated a gain-clamped erbium amplifier lasing at 1480 nm with the aid of narrowband grating reflectors, pumped at 980 nm.

The properties of all-optical gain-controlled amplifiers, pumped at 1480 nm, and lasing at longer wavelengths, have been studied by Massicott *et al.* [134]. The cavity configuration used for gain control, pumped at 1480 nm, is shown in Figure 8.30.

The amplifier cavity contains a length of erbium-doped fiber with two narrowband Bragg-matched fiber grating reflectors. Along with these gratings, a STG filter with a specified intracavity, loss is included close to the output end to control the intracavity loss and reduce the effect of stray reflections. Above a certain threshold pump power at which the cavity gain equals the intracavity loss, lasing occurs at a wavelength λ_1, clamping the gain across the gain bandwidth due to the homogeneous nature of the transition. With an increase in the pump power, energy is stored in the lasing flux, while maintaining the inversion, and therefore the gain. Signal wavelengths experience a fixed gain up to a certain critical input level, at the expense of the lasing flux. Once the input signal is large enough to extract all the energy from the lasing mode, the amplifier ceases to lase. Thereafter, the amplifier inversion (and gain) is uncontrolled and is dependent on the pump power and signal levels as for a normal erbium-doped fiber amplifier.

Figure 8.31 demonstrates the automatic optical gain controlled amplifier in operation. The amplifier consists of a 25-m length of erbium-doped fiber with a core diameter of 5.3 μm and refractive index difference of 0.013. The peak saturable absorption of the fiber is 6.1 dB/m with a background loss of 8 dB/km measured at a wavelength of 1.1 μm. The laser cavity is defined by two Bragg grating reflectors at 1520 nm, written in hydrogen-loaded GeO_2-SiO_2 fiber. The reflectivity of each grating is 94% with a 3-dB bandwidth of less than 0.4 nm. The splices dominate

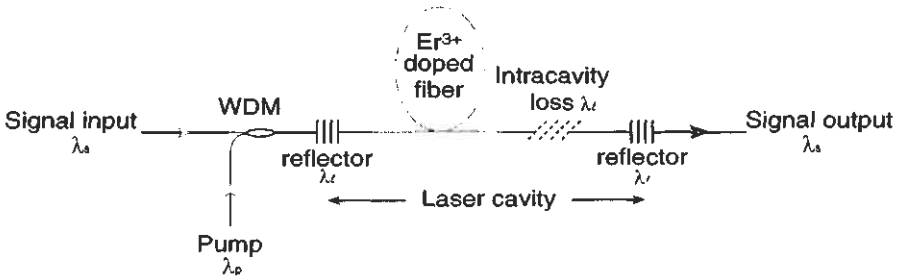


Figure 8.30: Amplifier with linear optical AGC.

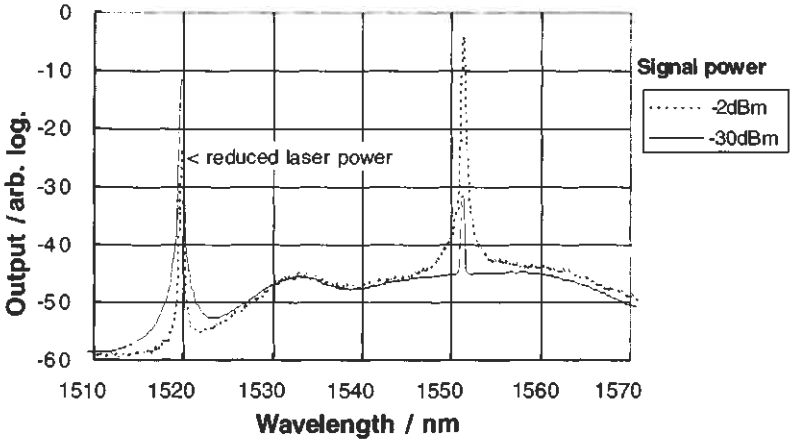


Figure 8.31: Output spectra of all-optical AGC amplifier, lasing at 1520 nm [134].

the cavity loss at 2.5 dB, single pass. The pump power in the fiber from a 1480-nm diode laser was approximately 80 mW.

Figure 8.31 shows the compensatory effect of the control laser in the broadband output spectra. As the input signal is increased to −2 dBm from the small signal level (−30 dBm), there is more than 10 dB of reduction in the residual laser output power. The inversion (and therefore the gain) in both cases remains the same. The excess noise in the high signal case is an artifact due to the side modes of the signal DFB source.

The evolution of the amplifier gain at 1550 nm, as a function of input signal level for four different pump powers is shown in Fig 8.32. A gain of nearly 16 dB is maintained up to an input signal power level of about −5 dBm, at the maximum pump power level of 80 mW.

The pump power no longer determines the amplifier's gain in the gain-controlled regime, only its maximum controlled output power. This is a desirable feature for a well-managed amplifier.

The dynamic performance of amplifiers with and without gain control is compared in Figs. 8.33 and 8.34. To test the transient response of the amplifiers an input signal of −10 dBm is modulated at 54 Hz and the outputs monitored on an oscilloscope, as shown in Fig. 8.33.

Without the signal present, the population inversion builds up in the uncontrolled amplifier. When the signal is injected, the output overshoots,

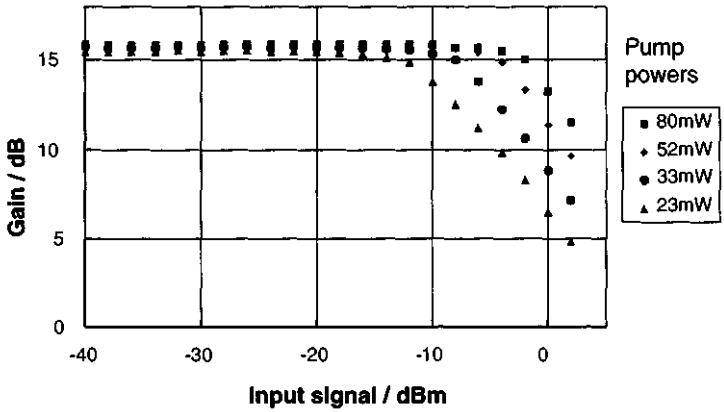


Figure 8.32: Gain characteristic of AGC amplifier. Lasing wavelength: 1520 nm; signal wavelength: 1550 nm; signal power: −30 dBm (from: Massicott J. F., Willson S. D., Wyatt R., Armitage J. R., Kashyap R., and Williams D., "1480nm pumped erbium doped fibre amplifier with all optical automatic gain control," *Electron. Lett.* **30**(12), 962–963, 1994. © IEE 1994, Ref. [134]).

producing a spike before a new equilibrium is reached. In the optical gain-controlled amplifier, the spike is eliminated.

Additionally, the induced cross-talk is also eliminated, as shown in Fig. 8.34. A small counterdirectionally propagating probe at 1560 nm is strongly affected in the uncontrolled amplifier but remains unaffected with AGC. In the absence of AGC, the CW probe output power more than doubles when the saturating signal is blocked, whereas in the controlled case, a change of less than 0.5% in output is seen.

To eliminate the residual laser power at 1520 nm, an additional STG [122] with a rejection of 30 dB is used. BER measurements performed at 2.5 Gb/sec show no penalty as a result of operating the amplifier in the optical gain-controlled regime.

A combination of both gain control and gain equalization forms a highly desirable amplifier. A GEQ filter composed of a concatenated set of STG filters, (as discussed in Section 8.8.1) added to the AGC amplifier output shows excellent GEQ-AGC. The flattened spectral shape is maintained for as long as the amplifier is operated within the gain-controlled range.

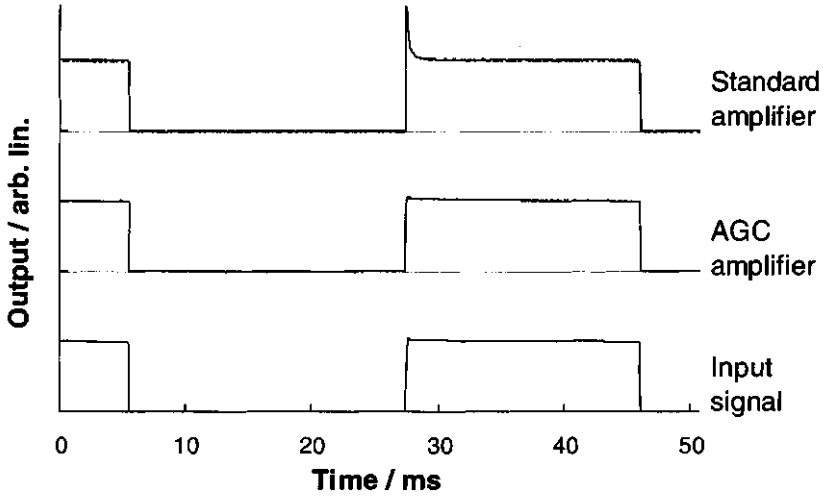


Figure 8.33: 1550-nm input signal modulated at 54 Hz (bottom trace), signal amplified using gain control (middle trace), and signal amplified without gain control (top trace) (from: Massicott J. F., Wilson S. D., Wyatt R., Armitage J. R., Kashyap R., and Williams D., "1480nm pumped erbium doped fibre amplifier with all optical automatic gain control," *Electron. Lett.* **30**(12), 962–963, 1994. © IEE 1994, Ref. [134]).

8.8.3 Analysis of gain-controlled amplifiers

For an amplifying fiber in which the Er^{3+} ion population inversion profile is approximated to be constant across the fiber core, the wavelength-dependent gain coefficient is given by

$$g_{(\lambda)} = \Gamma_{(\lambda)} N[(\sigma_{e(\lambda)} + \sigma_{a(\lambda)})n_2 - \sigma_{a(\lambda)}], \tag{8.8.1}$$

where $\sigma_{e(\lambda)}$ and $\sigma_{a(\lambda)}$ are the emission and absorption cross-sections, respectively, N is the axial Er^{3+} ion density, n_2 is the fraction of ions in the excited state, and $\Gamma_{(\lambda)}$ is the confinement factor representing the overlap between the propagating mode and the radial ion density distribution. In an amplifier in which gain control is in operation, the population inversion, and hence n_2, is set by the lasing condition, and amplifier gain calculations can be made without reference to the magnitudes of pump and signal power levels. The total linear loss at the laser cavity wavelength is

$$\text{Cavity loss} = e^{2g(las)L}. \tag{8.8.2}$$

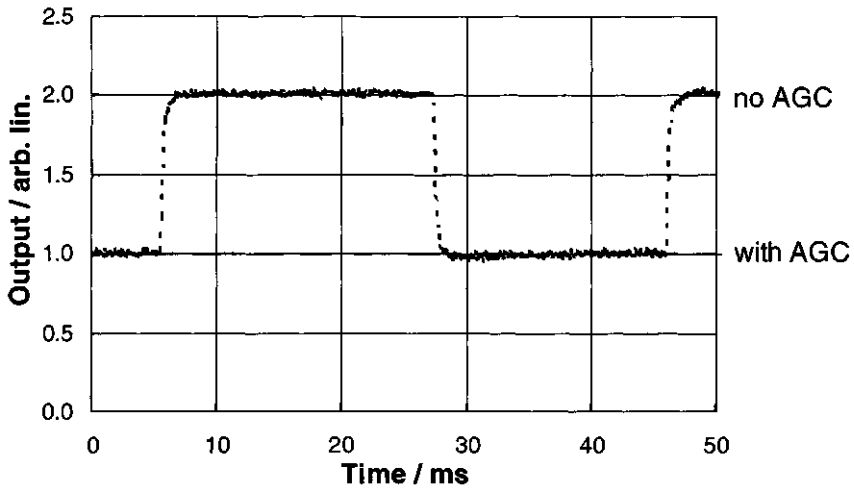


Figure 8.34: Cross-talk experienced by a contradirectionally propagating small signal 1560-nm probe to a modulated 1550-nm signal. Probe amplified using gain control (solid) and without gain control (dashed) [134].

Determination of the minimum required pump power to maintain gain control in the presence of signals of known magnitude is more involved. Approximate amplifier analyses (e.g., [135]) can be employed, but values so obtained substantially underestimate the actual power requirements. Principally, this is because no account is taken of pair induced quenching effects that degrade power conversion efficiencies even in low Er^{3+} ion concentration fibers [136].

8.8.4 Cavity stability

The gain stability of the amplifier is determined by the stability of the control laser wavelength and the laser cavity loss. The laser wavelength is fixed by the narrow-linewidth grating reflectors that have a temperature sensitivity of ~0.01 nm/°C. To avoid changes in cavity loss if drifting should occur, the use of one narrow- and one broader-band reflector is preferable. Reflections at the laser wavelength from other parts of the transmission system will alter the effective cavity loss, as will polarization dependence combined with birefringence in the fiber. The use of high-reflection gratings with an associated intracavity side-tap attenuator, as

opposed to reflectors of lower reflectivity, offers greater resilience to stray light from other parts of the transmission system.

8.8.5 Noise figure

The signal-spontaneous beat-noise figure for an amplifier is often given as

$$F_{(\nu)} = \frac{P^{sp}_{(\nu)}}{h\nu\delta\nu(G_{(\nu)} - 1)}, \tag{8.8.3}$$

where $P^{sp}_{(\nu)}$ is the spontaneous emission power at frequency ν, measured in a bandwidth $\delta\nu$. Over a length of fiber in which the population inversion is constant, the noise figure for that inversion can be calculated using

$$F_{(\lambda)} = 2\Big/\left(1 - \frac{\sigma_{a(\lambda)}}{\sigma_{e(\lambda)}}\frac{n_1}{n_2}\right). \tag{8.8.4}$$

It can be seen that for a given wavelength, the best noise figure is obtained for the highest possible inversion i.e., maximum n_2/n_1.

In a full-length amplifier, whether or not it is gain controlled, the local population inversion varies along the fiber length. The overall noise figure of the amplifier is predominantly determined at the signal input end [137], as spontaneous emission generated at the input experiences the full amplifier gain before being detected within the bandwidth of the signal receiver.

In an AGC amplifier, the evolution of the population inversion is, in part, determined by the laser power. For good overall noise performance, it is beneficial to minimize the laser power at the input in order to ensure that, as far as possible, the input inversion is determined by the shorter-wavelength pump source. This involves implementing as asymmetric a cavity configuration as possible. This is achieved by locating the bulk of the cavity loss at the signal output end of the amplifier and by choosing the wavelength of the control laser to be in a high-gain region of the spectrum requiring a correspondingly high cavity loss.

Figure 8.35 shows the measured gain and noise figures of an AGC amplifier with a linear control laser cavity at 1530 nm [138]. The pump and signal powers are referenced to the input and output of the doped fiber and the measured noise figures are compared with data obtained using a full numerical amplifier model [139]. In one case the cavity loss

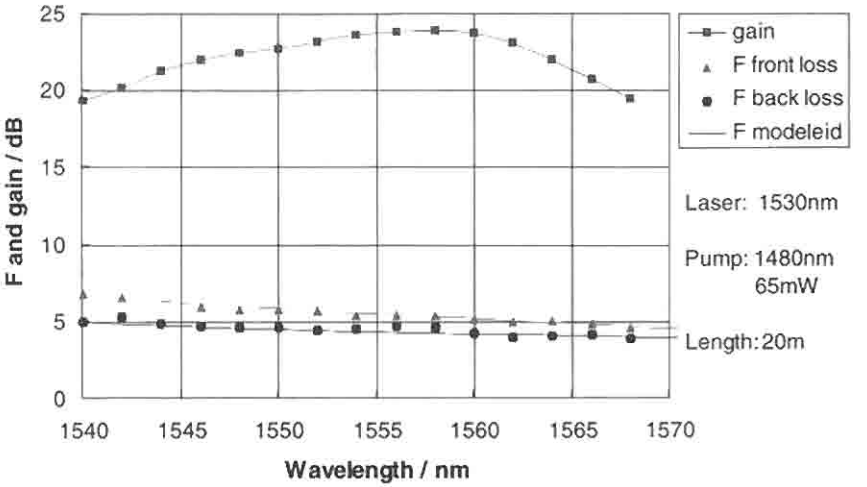


Figure 8.35: Gain and noise figure for an AGC amplifier in two cavity implementations (courtesy J. Massicott, BT Laboratories).

grating is placed at the front end of the cavity, and in the other, at the back. The gain spectra for the two cases were identical to within experimental error, but the expected noise figure improvement is achieved when the cavity loss is located at the signal output end of the laser cavity.

References

1 Betti S., De Marchais G., and Iannone E., *Coherent Optical Communications System*, Wiley, New York (1995).

2 Olsson A. and Tang C. L., "Coherent optical interference effects in external cavity semiconductor lasers," *IEEE J. Quantum Electron.* **QE-17**, 1320–1323 (1981).

3 Tkach R. W. and Chraplyvy A. R., "Regimes of feedback effects in 1.5 μm distributed feedback laser," *J. Lightwave Technol.* **LT-4**, 1655–1661 (1986).

4 Wyatt R. and Devlin W. J., "10kHz linewidth 1.5 μm, InGaAsP external cavity laser with 55nm tuning range," *Electron. Lett.* **19**, 110–112 (1983).

5 Olsson N. A., Henry C. H., Kazarinov R. F., Lee H. J., and Orlowsky K. J., "Performance characteristics of a 1.5 μm single frequency semiconductor

laser with an external waveguide Bragg reflector," *IEEE J. Quantum Electron.* **QE-43**, 143–147 (1988).

6 Meltz G. and Morey W. W., "Bragg grating formation and germanosilicate fiber photosensitivity," *SPIE* **1516**, International Workshop on Photo-induced Self-Organisation effects in Optical Fibres," p. 185 (1991).

7 ITU-T specification of wavelength for WDM.

8 Adams M. J., Steventon A. J., Devlin W., and Henning I., *Semiconductor Lasers for Long Wavelength Optical Fibre Communication Systems,* Peter Peregrinus (1987).

9 Osinski M. and Buus J., "Linewidth broadening factor in semiconductor lasers — an overview," *IEEE J. Quantum. Electron.* **QE-23**(1), 9–21 (1987).

10 Olsson N. A., Henry C. H., Kazarinov R. F., Lee H. J., and Johnson B. H., "Relation between chirp and linewidth reduction in external Bragg reflector semiconductor laser," *Appl. Phys. Lett.* **47**, 183–185 (1985).

11 Timofeev F. N., Bayvel P., Reekie L., Tucknott J., Midwinter J. F., and Payne D. N., "Spectral characteristics of a reduced cavity single mode semiconductor fiber grating cavity for applications in dense systems," in *Proc. of 21st European Conf. Optic. Commun., ECOC'95*, Brussels, Belgium, paper TuP. 26, pp. 477–480 (1995).

12 Brinkmeyer E., Brennecke W., Zürn M., and Ulrich R., "Fiber Bragg reflector for mode selection and line-narrowing of injection lasers," *Electron. Lett.* **22**(3), 134–135 (1986).

13 Park C. A., Rowe C. J., Buus J., Reid D. C. J., Carter A., and Bennion I., "Single-mode behaviour of a multimode 1.55 μm laser with a fiber grating external cavity," *Electron. Lett.* **22**, 1132–1134 (1986).

14 Morey W. W., Meltz G., and Glenn W. H., "Fiber optic Bragg grating sensors," SPIE **1169,** *Fiber optics Sensors VII*, pp. 98–107 (1989).

15 Bird D. M., Armitage J. R., Kashyap R., Fatah R. M. A., and Cameron K. H., "Narrow line semiconductor laser using fiber grating," *Electron. Lett.* **27**, 1115 (1991).

16 Williams D. L., Ainslie B. J., Kashyap R., Sherlock G., Smith R. P., and Collins J. V., "Temperature stable 1.3 μm laser with Bragg fiber grating external cavity for access networks," in *Proc of ECOC'93*, pp. 209–212 (1993).

17 Morton P. A., Mizrahi V., Lemaire P. J., Tanbun-Ek, Logan R. A., Presby H. M., Erdogan T., Woodward S. L., Phillips M. R., Sargent A. M., and Wecht K. W., "High power narrow-linewidth stable single-mode hybrid," in *Proc. Conference on Optical Fiber Communications, OFC'94 Technical Digest*, Paper WG4, p. 102 (1994).

18 Morton P. A., Mizrahi V., Tanbun-Ek, Logan R. A., Lemaire P. J., and Presby, H. M., "Stable single mode hybrid laser with high power and narrow linewidth," *Appl. Phys. Lett.* **64**, 2634–2636 (1994).

19 Edwards C. A., Presby H. M., and Stulz L. W., "Effective reflectivity of hyperbolic micro lenses," *Appl. Opt* **32**, 2099 (1993).

20 Giles C. R., Erdogan T., and Mizrahi V., "Simultaneous wavelength stabilisation of 980nm pump lasers," *IEEE Photon. Technol. Lett.* **6**, 907–909 (1994).

21 Ventrudo B. F., Rogers G. A., Lick G. S., Hargreaves D., and Demayo T. N., "Wavelength and intensity stabilisation of 980nm diode lasers coupled to fiber Bragg gratings," *Electron. Lett.* **30**(25), 2147–2149 (1994).

22 Petermann K., in *Laser Diode Modulation and Noise,"* Chapter 7. Kluwer Academic Publishers, Dordrecht (1991).

23 Pan J. J., Jing X. L., and Shi Y., "Fiber grating stabilized source for dense WDM systems," in *Proc. of Optical Fiber Conf., OFC'97*, paper WL48, p. 213.

24 Campbell R. J., Armitage J. R., Sherlock G., Williams D. L., Smith R. P., Robertson M. J., and Wyatt R., "Wavelength stable uncooled fiber grating semiconductor laser for use in an all optical WDM access network," *Electron. Lett.* **32**, 119–120 (1996).

25 Collins J. V., Lealman I. F., Fiddyment P. J., Jones C. A., Waller R. G., Rivers L. J., Cooper K., Perrin S. D., Neild M. W., and Harlow M. J., "Passive alignment of a tapered laser with more than 50% coupling efficiency," *Electron Lett.* **31**(9), 730–731 (1995).

26 Kashyap R., Payne R., Whitley T., and Sherlock G., "Wavelength uncommitted lasers," *Electron. Lett.* **30**(13), 1065 (1994).

27 Timofeev F. N., Bayvel P., Midwinter J. E., Wyatt R., Kashyap R., and Robertson M., "2.5Gbit/s dense WDM, transmission in standard fibre using directly modulated fibre grating lasers," *Electron Lett.* **33**(19), 1632–1633 (1997).

28 Timofeev F. N., Bayvel P., Mikhailov V., Gambini P., Wyatt R., Kashyap R., Robertson M., Campbell R. J., and Midwinter J. E., "Low chirp, 2.5 Gbit/s directly modulated fibre grating laser for WDM networks," in *Technical Digest of Conf. on Opt. Fib. Commun., OFC'97*, p. 296 (1997).

29 Timofeev F. N., Bayvel P., Midwinter J. E., Wyatt R., Kashyap R., and Robertson M., "2.6 Gbit/s dense WDM transmission in standard fibre using directly modulated fibre grating lasers," *Electron Lett.* **33**(19), 1632–1633 (1997).

30 Timofeev F. N., Bayvel P., Mikhailov V., Lavrova O. A., Wyatt R., Kashyap R., Robertson M., and Midwinter J. E., "2.5 Gbit/s directly modulated fibre grating laser for WDM network," *Electron. Lett.* **33**(16), 1406–1407 (1997).

31 Timofeev F. N., Bennett S., Griffin R., Bayvel P., Seeds A., Wyatt R., Kashyap R., and Robertson M., "High spectral purity millimetre-wave modulated opti-

cal signal generation using fibre grating lasers," *Electron. Lett.* **34**(7), 668–669 (1998).

32 Paoletti P., Meliga M., Oliveti G., Puleo M., Rossi G., and Senepa L., "10 Gbit/s ultra low chirp 1.55 μm directly modulated hygrid fiber grating semiconductor laser source," in *Tech. Digest of ECOC'97*, pp. 107–110 (1997).

33 Premaratne M., Lowery A. J., Ahmed Z., and Novak D., "Modelling noise and modulation performance of fiber Bragg grating external cavity lasers," *IEEE J. Selected Topics in Quantum Electron.* **3**(2), 290–303 (1997).

34 Park J. D., Seo D. S., and McInerney J. G., "Self-pulsation in strongly coupled asymmetric external cavity semiconductor lasers, *IEEE J. Quantum Electron.* **26**, 1353–1362 (1990).

35 Rong-Qing H. and Shang-Ping T., "Improved rate equations for external cavity semiconductor lasers," *IEEE J. Quantum. Electron.* **25**, 11580–1584 (1989).

36 Berger O., "Dynamische Modellierung von Fasergitterlasern für optoelektronische Mikrowellenerzeugung," Diplomarbeit, Universität Duisberg (1998).

37 Morton P. A., Mizrahi V., Kosinski S. G., Mollenauer L. F., Tanbun-Ek T., Logan R. A., Coblentz D. L., Sargent A. M., and Wecht K. W., "Hybrid soliton pulse source with fibre external cavity and Bragg reflector," *Electron. Lett.* **28**(6), 561 (1992).

38 Morton P. A., Mizrahi V., Andrekson P. A., Tanbun-Ek T., Logan R. A., Lemaire P., Coblentz D. L., Sargent A. M., Wecht K. W., and Sciortino P. F., Jr. "Mode locked hybrid soliton pulse source with extremely wide operating frequency range," *IEEE Photonics Tech. Lett.* **5**(1), 28 (1993).

39 Ahmed Z. and Tucker R. S., "Small-signal IM response of grating-terminated external cavity semiconductor lasers," *IEEE J. Selected Topics in Quantum Electron.* **1**, 505–515 (1995).

40 Tomita A. and Suzuki A., "Optical feedback effect on bistable laser diodes," *Opt. Quantum Electron.* **15**, S75–S82 (1987).

41 Snitzer E. and Koester C. J., "Amplification in a fiber laser," *Appl. Opt.* **3**, 1182–1186 (1964).

42 Ainslie B. J., Beales K. J., Cooper D. M., Day C. R., and Rush J. D., "Monomode fibre with ultra-low loss and minimum dispersion at 1.55 μm," *Electron. Lett.* **18**, 842–844, 1982.

43 See, for example, *Optical Fiber Lasers and Amplifiers* (France P. W., Ed.). Blackie and Sons, London (1991).

44 Øbro M., Pedersen J. E., and Brierley M. C., "Gain enhancement in Nd^{3+} doped ZBLAN fibre amplifier using mode coupling filter," *Electron. Lett.* **28**(1), 99–100 (1992).

45 Miller I. D. and Hunt M. H., "Optical fibre locating apparatus ," UK Patent no. 89301940, 27 February 1989.

46 Jauncey I. M., Reekie L., Mears R. J., Payne D. N., Rowe C. J., Reid D. C. J., Bennion L., and Edge C., "Narrow-linewidth fiber laser with integral fiber grating," *Electron. Lett.* **22**(19), 987–988 (1986).

47 Wyatt R., "High power broadly tunable erbium-doped silica fiber laser," *Electron. Lett.* **25**(22), 1498–1499 (1989).

48 Kashyap R., Armitage J. R., Wyatt R., Davey S. T., and Williams D. L., "All-fiber narrowband reflection gratings at 1500 nm, *Electron. Lett.* **26**(11), 730 (1990).

49 Ball G. A., Morey W. W., and Waters J. P., "Nd^{3+} fiber laser utilising intra-core Bragg reflectors," *Electron Lett* **26**(21), 1829 (1990).

50 Mizrahi V., DiGiovanni D., Atkins R. M., Park Y., and Delavaux J-MP "Stable single-mode erbium fiber grating laser for digital communication," *IEEE J. Lightwave Technol.* **11**(12), 2021 (1993).

51 Zyskind J. L., Mizrahi V., DiGiovanni D. J., and Sulhoff J. W., "Short single-frequency Erbium-doped fiber laser," *Electron. Lett.* **28**, 1385 (1992).

52 Chernikov S. V., Kashyap R., McKee P. F., and Taylor J. R., "Dual frequency all fiber grating laser source," *Electron Lett.* **29**(12), 1089 (1993).

53 Chernikov S. V., Taylor J. R., and Kashyap R., "Coupled-cavity erbium fiber lasers incorporating fiber grating reflectors," *Opt. Lett.* **18**(23), 2023, 1993, and Chernikov S. V., Taylor J. R., and Kashyap R., "Integrated all optical fiber source of multigigahertz soliton pulse train," *Electron. Lett.* **29**(20), 1788 (1993).

54 Ball G. A., Morey W. W., and Cheo P. K., "Single- and multipoint fiber-laser sensors," *IEEE Photonics Tech. Lett.* **5**(2), 267 (1993).

55 Ball G. A. and Morey W. W., "Narrow-linewidth fiber laser with integrated master oscillator-power amplifier," *Proc. Conference on Optical Fiber Communications, OFC'92*, p. 97 (1992).

56 Archambault J. L. and Grubb S. G., "Fiber gratings in lasers and amplifiers," *J. Lightwave Technol.* **15**(8), 1378–1390 (1987).

57 Loh W. H., Laming R. I., and Zervas M. N., "Single frequency erbium fiber external cavity semiconductor laser," *Appl. Phys. Lett.* **66**(25), 3422–3424 (1995).

58 Grubb S. G., "High power fiber amplifiers and lasers" in *Proc. of OFC'95*, Tutorial Session (1996).

59 SDL FL-10, SDL Inc., 80 Rose Orchard Way, San Jose, CA. USA.

60 Digonnet M. J. F., "Closed-form expressions for the gain in three- and four-level laser fibers," *IEEE J. Quantum Electron.* **26**, 1788–1796 (1990).

61 Ball G. A. and Glenn W. H., "Design of a single-mode linear-cavity erbium fiber laser utilising Bragg reflectors," *J. Lightwave Technol.* **10**(10), 1338 (1992).

62 Ball G. A., Glenn W. H., Morey W. W., and Cheo P. K., "Modelling of short, single-frequency, fiber lasers in high-gain fiber," *IEEE Photonics Tech. Lett.* **5**(6), 649 (1993).

63 Le Boudec P., Francois P. L., Delevaque E., Bayon J.-F., Sanchez E., and Stephan G. M., "Influence of ion pairs on the dynamical behaviour of Er^{3+} doped fiber lasers," *Opt. & Quantum. Electron.* **25**, 501 (1993).

64 Ball G. A., Hul-Allen G., Holton C. E., and Morey W. W., "Low noise single frequency linear fibre laser," *Electron. Lett.* **29**, 1623–1625 (1993).

65 Kane T. J., "Intensity noise in diode-pumped single-frequency Nd:YAG lasers and its control by electronic feedback," *IEEE Photon. Technol. Lett.* **2**(4), 244–245 (1990).

66 Zyskind J. L., Sulhoff J. W., Magill P. D., Reichmann K. C., Mizrahi V., and DiGiovanni D. J., "Transmission at 2.5 Gbit/s over 654 km using an erbium-doped fiber grating laser source," *Electron. Lett.* **29**(12), 1105 (1993).

67 Delavaux J.-M. P., Park Y. Y., Mizrahi V., and DiGiovanni D. J., "Long term bit error rate transmission using an erbium fiber grating laser transmitter at 5 and 2.5 Gb/s," in *Tech. Proc. of ECOC'93*, paper TuC3.3, pp. 69–71 (1993).

68 Ball G. A., Hul-Allen G., Holton C. E., and Morey W. W., "60 mW 1.5 μm single-frequency low noise fibre laser MOPA," *IEEE Photon. Technol. Lett.* **6**(2), 192–194 (1994).

69 Kringlebotn J. T., Archambault J. L., Reekie L., Townsend J. E., and Payne D. N., "Highly-efficient, low-noise grating-feedback Er^{+3}:Yb^{3+} codoped fibre laser," *Electron. Lett.* **30**(12), 972–973 (1994).

70 Kringlebotn J. T., Morkel P. R., Reekie L., Archambault J. L., and Payne D. N., "Efficient diode-pumped single frequency erbium:ytterbium fibre laser," *IEEE Photonics Technol. Lett.* **5**(10), 1162 (1993).

71 Allain J. Y., Bayon J.-F., and Monerie M., "Ytterbium-doped silica fiber laser with intracore Bragg gratings at 1.02 μm," *Electron. Lett.* **29**, 309 (1993).

72 Coldren L. A., Millar B. I., Iga K., and Rentschler J. A., "Monolithic two-section GaInsAsP/InP active optical resonator devices formed by reactive ion etching," *Appl. Phys. Lett.* **38**, 315 (1981).

73 Tsang W. T., Olsson N. A., and Logan R. A., "High speed direct single-frequency modulation with large tuning rate and frequency excursion in cleaved coupled cavity semiconductor laser," *Appl. Phys. Lett.* **42**, 650 (1983).

74 Lang R. J., Yariv A., and Salzman J., "Laterally coupled cavities semiconductor lasers," *IEEE J. Quantum Electron.* **QE-23**, 395 (1987).

75 Dianov E. M. and Okhotnikov O. G., *Sov. Lightwave Commun.* **2**, 823 (1992).

76 Pan J. J. and Shi Y., "Tunable Er^{+3}-doped fibre ring laser using fibre grating incorporated by optical circulator or fibre coupler," *Electron. Lett.* **31**(14), 1164–1165 (1995).

77 Guy M. J., Taylor J. R., and Kashyap R., "Single-frequency erbium fibre ring laser with intracavity phase-shifted fibre Bragg grating narrowband filter," *Electron. Lett.* **31**(22), 1924–1925 (1995).

78 Yun S. H., Richardson D. J., Culverhouse D. O., and Kim B. Y., "Wavelength-swept fiber laser with frequency-shifted feedback," in *Tech. Digest of OFC'97*, pp. 30–31 (1997).

79 Dong L., Loh W. H., Caplen J. E., Hsu K., Minelli J. D., and Reekie L., "Photosensitive Er/Yb optical fibers for efficient single-frequency fiber lasers," in *Tech. Digest of OFC'97*, pp. 29–30 (1997).

80 Dong L., Loh W. H., Caplen J. E., Hsu K., Minelli J. D., and Reekie L., "Efficient single-frequency fiber lasers with novel photosensitive Er/Yb optical fibers," *Opt. Lett.* **22**(10), 694–696 (1997).

81 Utaka K., Akiba S., and Matsushima Y., "$\lambda/4$-shifted GaAsP/InP DFB lasers by simultaneous holographic exposure of negative and positive photoresists," *Electron. Lett.* **20**, 1008–1010 (1984).

82 Asseh H., Storoy H., Kringlebotn J. T., Margulis W., Sahlgren B., and Sandgren S., "10 cm long Yb^{+} DFB fibre laser with permanent phase shifted grating," *Electron. Lett.* **31**, 969–970 (1995).

83 Sejka M., Varming P., Haübner J., and Kristensen M., "Distributed feedback Er^{+3} doped fibre laser," *Electron. Lett.* **31**(17), 1445–1446 (1995).

84 Loh W. H. and Laming R. I., "1.55 μm phase-shifted distribute feedback fibre laser," *Electron. Lett.* **31**(17), 1440–1442 (1995).

85 Hübner J., Varming P., and Kristensen M. "Five wavelength DFB fibre laser source for WDM systems," *Electron. Lett.* **33**(2), 139–140 (1997).

86 Lauridsen V. C., Sondergaard T., Varming P., and Povlsen J. H., "Design of distributed feedback fiber lasers," *In Proc. of ECOC'97*, Vol. 3, pp. 39–42 (1997).

87 Graydon O., Loh W. H., Laming R. I., and Dong L., "Triple-frequency operation of an Er-doped twin-core fiber loop laser," *IEEE Photon. Technol. Lett.* **8**(1), 63–65 (1996).

88 Ball G. A. and Morey W. W., "Continuously tuneable single-mode erbium fiber laser," *Opt. Lett.* **17**(6), 420 (1992).

89 Ball G. A. and Morey W. W., "Compression-tuned single-frequency Bragg grating fiber laser," *Opt. Lett.* **19**(23), 1979–1981 (1994).

90 Hsu K., Loh W. H., Dong L., and Miller C. M., "Efficient and tunable Er/Yb fiber grating lasers," *J, Lightwave Technol.* **15**(8), 1438–1441 (1997).

91 Gunning P., Kashyap R., Siddiqui A. S., and Smith K., "Picosecond pulse generation of <5 ps from gain-switched DFB semiconductor laser diode using a linearly ste-chirped grating," *Electron. Lett.* **31**(13), 1066–1067 (1995).

92 Eggleton B. J., Krug P. A., Poladin L., Ahmed K. A., and Liu J.-F., "Experimental demonstration of compression of dispersed optical pulses by reflection from a self-chirped optical fiber Bragg grating," *Opt. Lett.* **19**, 877–879 (1994).

93 Chernikov S. V., Taylor J. R., and Kashyap R., "Comblike dispersion-profiled fiber soliton pulse train generation," *Opt. Lett.* **19**(8), 539–541 (1994).

94 Davey R. P., Fleming R. P. E, Smith K., Kashyap R., and Armitage J. R., "Mode-locked erbium fibre laser with wavelength selection by means of a fibre Bragg grating reflector," *Electron. Lett.* **27**(22), 2087–2088 (1991).

95 Ahmed K. A., Eggleton B. J., Liu H. F., Krug P. A., and Ouellette F., "Simultaneous mode-selection and pulse compression of gain switched pulses from a Fabry–Perot laser using a 40 mm chirped optical fiber grating," *IEEE Photon. Technol. Lett.* **7**, 158–160 (1995).

96 Karpman V. I. and Solov'ev V. V., "A perturbational approach to the two-soliton systems," *Physica D*(3), 487–502 (1981).

97 Mollenauer L. F., Evangelides S. G., and Haus H. A., "Long distance solution propagation using lumped amplifiers and dispersion shifted fiber," *IEEE J. Lightwave Technol.* **9**, 194 (1991).

98 Chernikov S. V., Dianov E. M., Richardson D. J., Laming R. I., and Payne D. N., "114 Gb/s soliton train generation through Raman self scattering of a dual frequency beat signal in dispersion decreasing optical fiber," *Appl. Phys. Lett.* **63**, 293–295 (1993).

99 Mamyshev P. V., Chernikov S. V., and Dianov E. M., "Generation of fundamental soliton trains for high-bit rate optical fibre communication lines," *IEEE J. Quantum. Electron.* **27**, 2347–2355 (1991).

100 Kashyap R., Chernikov S. V., and Taylor J. R., "Fibre laser and beat frequency sources based on fibre gratings for microwave and ultrafast processing," *Int. J. Optoelectron.* **11**(2), 87–92 (1997).

101 Chernikov S. V., Kashyap R., Guy M. J., Moodie D. G., and Taylor J. R., "Ultrahigh-bit-rate optical sources and application," *Phil. Trans. R. Soc. Lond. A* **354**, 719–731 (1996).

102 Noske D. U., Guy M. J., Rottwitt K., Kashyap R., and Taylor J. R., "Dual-wavelength operation of a passively mode-looked 'figure-of-eight' ytterbium-erbium fibre soliton laser," *Opts. Comm.* **108**, 297–301 (1994).

103 Pataca D. M., Rocha M. L., Kashyap R., and Smith K., "Bright and dark pulse generation in an optically mode-locked fibre laser at 1.3 mm," *Electron. Lett.* **31**(1), 35–36 (1995).

104 Woodbury E. J. and Ng W. K., "Ruby laser operation in the near IR", *Proc. IRE 50,* 2347, 1962.

105 See, for example, Shen Y. R., *The Principles of Nonlinear Optics*. Wiley, New York (1984).

106 Stolen R. H., "Nonlinearity in fiber transmission," *Proc. IEEE* **68**(10), 1232–1236 (1980).

107 Akoi Y., "Properties of fiber Raman amplifiers and their applicability to digital optical communication systems," *Lightwave Technol.* **6**, 1225 (1988).

108 Hill K. O., Kawasaki B. S., and Johnson D. C., "CW Brillouin laser," *Appl. Phys. Lett.* **28**, 608 (1976).

109 Jain R. K., Chinlon Lin, Stolen R. H., Pleibel W., and Kaiser P., "A high-efficiency tunable cw Raman oscillator," *Appl. Phys. Lett.* **30**(3), 162–164 (1977).

110 Stolen R. H., Chinlon Lin, and Jain R. K., "A time-dispersion-tuned fiber Raman oscillator," *Appl. Phys. Lett.* **30**(7), 340–342 (1977).

111 Stolen R. H. and Lin C., "Fiber Raman lasers," in *CRC Handbook of Laser Science and Technology, Supplement I: Laser*, CRC Press (1991).

112 Grubb S. G., "High power diode-pumped fiber lasers and amplifiers," in *Proc. of OFC'95*, paper TuJ1, pp. 41–42 (1995).

113 Grubb S. G., "High power 1.48 μm cascaded Raman laser in germanosilicate fiber," in *OFC'95, the Conference on Optical Communication*, Vol. 8, 1995 Technical Digest Series, Postconference Edition, pp. 41–42 (1995).

114 Dianov E. M., Abramov A. A., Bubnov M. M., Shipulin A. V., Prokhorov A. M., Semjonov S. L., and Schebunjaev, "Demonstration of 1.3 μm Raman fiber amplifier gain os 25 dB at a pumping power of 300 mW," *Opt. Fib. Technol.* **1**, 236–238 (1995).

115 Grubb S. G., Erdogan T., Mizrahi V., Strasser T., Cheung W. Y., Reed W. A., Lemaire P. J., Miller A. E., Kosinski S. G., Nykolak G., and Becker P. C., "1.3 μm cascaded Raman amplifier in germanosilicate fibers," in *Proc. of OAA'94*, paper PD3 (1994).

116 Desurvire E., Chapter 2, pp. 108, in *Erbium Doped Fiber Amplifiers*. Wiley, New York (1994).

117 Stentz A. J., Nielsen T., Grubb S. G., Strasser T. A., and Pedrazzani J. R., "Raman ring amplifier at 1.3 μm with analog-grade noise performance and output power of 23 dBm," in *Proc. of OFC'96*, paper PD16, pp. 391–394 (1996).

118 Hansen P. B., Stentz A. J., Eskilden L., Grubb S. G., Strasser T. A., and Pedrazzani J. R., "High sensitivity 1.3 μm optically pre-amplified receiver using Raman amplification," *Electron. Lett.* **32**(23), 2164–2165 (1996).

119 Nakazawa M., Yamada E., Kubota H., and Suzuki K., "10 Gb/s soliton data transmission over 1 million kilometers," *Elec. Lett.* **27**, 1270–1272 (1991).

120 Hill G. R., Fernandes L., and Cadeddu R., "Building the road to optical networks," *Br. Telecom. Engg.*, **16**, 2–12 (1997).

121 Kashyap R., Wyatt R., and Campbell R. J., "Wideband gain flattened erbium fibre amplifier using a photosensitive fibre blazed grating," *Electron. Lett.* **29**(2), 154–155 (1993).

122 Kashyap R., Wyatt R., and McKee P. F., "Wavelength flattened saturated erbium amplifier using multiple side-tap Bragg gratings," *Electron. Lett.* **29**(11), 1025–1026 (1993).

123 Kashyap R., unpublished (1993).

124 Holmes M. J., Kashyap R., Wyatt R., and Smith R. P., "Development of radiation mode filters for WDM," in *Proc. of IEE Symposium on WDM Technology*, IEE, 16–17 (June 1998).

125 Dianov E. M., Karpov V. I., Kurkov A. S., Medvedkov O. I., Prokhorov A. M., Protopopov V. N., and Vasil'ev S. A., "Gain spectrum flattening of erbium doped fiber amplifier using long period grating," in *Photosensitivity and Quadratic Nonlinearity in Glass Waveguides: Fundamentals and Applications*, Vol. 22, 1995 OSA Technical Series (Optical Society of America, Washington, DC, 1995), pp. SbB3-(14–17) (1995).

126 Vengsarkar A. M., Pedrazzani J. R., Judkins J. B., Lemaire P. J., Bergano N. S., and Davidson C. R., "Long-period fiber grating based gain equalisers," *Opt. Lett.* **21**, 336–338 (1996).

127 Ellis A. D., Percival R. M., Lord A., and Stallard W. A., "Automatic gain control in cascaded erbium-doped fibre amplifier systems," *Electron. Lett.* **3**, 193 (1991).

128 Bayart D., Clesca B., Hamon I., and Beylat J. L., "1.55 μm fluoride-based EDFA with gain-flatness control for multiwavelength applications," *Electron. Lett.* **17**, 1407 (1994).

129 Motoshima K., Leba L. M., Chen D. N., Downs M. M., Li T., and Desurvire E., "Dynamic compensation of transient gain saturation in erbium-doped fibre amplifiers by pump feedback control," *IEEE Photon. Technol. Lett.* **12**, 1423 (1993).

130 Desurvire E., Zirngible M., Presby H. M., and DiGiovanni D., "Dynamic gain compensation in saturated erbium-doped fibre amplifiers," *IEEE Photon Technol. Lett.* **5**, 453 (1991).

131 Motoshima K., Shimizu K., Takano K., Mizuochi T., and Kitayama T., "EDFA with dynamic gain compensation for multiwavelength transmission systems," *OFC'94 Technical Digest*, 191 (1994).

132 Zirngibl M., "Gain control in erbium-doped fibre amplifiers by an all-optical feedback loop," *Electron. Lett.* **27**(7), 560–561 (1991).

133 Delevaque E., Georges T., Bayon J. F., Monerie M., Niay P., and Berage, P., "Gain control in erbium-doped fibre amplifiers by lasing at 1480 nm with photoinduced Bragg gratings written on the fibre ends," *Electron. Lett.* **29**(12), 1112–1113 (1993).

134 Massicott J. F., Willson S. D., Wyatt R., Armitage J. R., Kashyap R., and Williams D., "1480 nm pumped erbium doped fibre amplifier with all optical automatic gain control," *Electron. Lett.* **30**(12), 962–963 (1994).

135 Saleh A. A. M., Jopson R. M., Evankow J. D., and Aspell J., "Modeling of gain in erbium-doped fibre amplifiers," *IEEE Photon. Technol. Lett.* **2**(10), 714 (1990).

136 Georges T., Delevaque E., Monerie M., Lamouler P., and Bayon J. F., "Pair induced quenching in erbium doped silicate fibers," *IEEE Optical Amplifiers and Their Applications, Technical Digest*, Vol. 17, p. 71 (1992).

137 Olshansky R., "Noise figure for erbium-doped optical amplifiers," *Electron. Lett.* **24**(22), 1363–1365 (1988).

138 Massicott J. F., Lebre C., Wyatt R., Kashyap R., Williams D., and Yu A., "Low noise, all-optical gain controlled Er3+ doped fibre amplifier using asymmetric control laser cavity design," *Electron. Lett.* **32**(9), 816–817 (1996).

139 Yu A. and O'Mahony M. J., "Properties of gain controlled erbium doped fibre amplifiers by lasing," *Electron Lett.* **31**(16), 1348 (1995).